April 2018

Inorganic Nanowire-Modified Polyelectrolytes for Vanadium Flow Battery Membranes

Brandon David Clark
Worcester Polytechnic Institute

Inorganic Nanowire-Modified Polyelectrolytes for Vanadium Flow Battery Membranes

A Major Qualifying Project
Submitted to the Faculty of
Worcester Polytechnic Institute
in partial fulfillment of the requirements for the
Degrees in Bachelor of Science
in
Chemical Engineering
and
Electrical and Computer Engineering
By

Brandon Clark

Date: 4/24/18

Project Advisors:

Dr. Amy Peterson

Dr. Yousef Mahmoud

Abstract

Vanadium redox flow batteries (VRFBs) are seen as promising candidates for renewable energy storage due to their nearly unlimited storage capacity, hindered only by the size of the tank that holds their electrolyte solution. However, the high cost of the battery's ion-exchange membrane, DuPont's Nafion, restricts the battery's economic viability for widespread installation. Nafion also exhibits high vanadium permeability over time, which severely hinders battery lifespan. Studies show that Nafion conducts protons well because of the natural 4 nm sulfonate ion channels it forms, but these channels might also be large enough for vanadium ions. To this end, it was hypothesized that simpler polyanions, when casted with inorganic nanowires, would order themselves around the nanowires, thereby orienting charged channels for proton mobility while simultaneously plugging most of their volume from vanadium bulk transport. This project represents an initiative to replace Nafion with a low cost vanadium redox flow battery membrane with high selectivity and conductivity.

In this project, the self-assembly behavior of PSS (Polystyrene sulfonate) and zinc oxide (ZnO) nanowires were studied in aqueous solution using dynamic light scattering. These two materials were then casted as composite films, and their thermomechanical properties compared to pure PSS films were analyzed using dynamic mechanical analysis. Finally, in order to create a membrane that was insoluble in aqueous battery solutions, multiple crosslinking reactions were attempted to create a chemically stable membrane resin. In parallel to membrane studies, a battery prototype was designed and built in order to prepare for future membrane charge/discharge load testing. In order to record battery voltage and current during these experiments, an original data collection apparatus was built using the Particle Photon, a WIFI-enabled embedded computer. Battery transient analysis was then conducted using a commercial Nafion membrane.

Dynamic light scattering measurements suggested that PSS readily electrostatically interacts with ZnO nanowires in a way that might create ion channels. Dynamic mechanical analysis data should no clear trend, but more tests need to be run to confirm ZnO's effect on membrane mechanical properties. The only crosslinking strategy that showed promise was using glutaraldehyde to crosslink poly(allylamine hydrochloride) across PSS in a polyelectrolyte complex. This crosslinked complex successfully did not dissolve in water, but it did swell considerably, thus losing most mechanical strength and splitting upon the application of moderate manual force. New reaction conditions need to be explored to mitigate swelling and prevent membrane splitting. Thankfully, the prototype battery proved to charge and discharge vanadium solutions very consistently. However, a very high internal resistance causes an extremely low coulombic efficiency of around 5%. Higher quality electrode materials and thinner internal flow frames are hypothesized to mitigate this. Overall, this project provides crucial steps for future research into the fabrication, characterization, and performance testing of low cost vanadium redox flow battery membranes.

Acknowledgements

This work was funded by the WPI departments of Chemical Engineering and Electrical and Computer Engineering. I would like to thank Dr. Amy Peterson, Dr. Yousef Mahmoud, Ivan Ding, Anthony D'Amico, and Xuejian Lyu for their support and mentorship.

Table of Contents

List of Figures

1. Introduction

In order to preserve global environmental health while supporting future societal energy needs, it is necessary for solar and wind energy to overcome fossil fuels as the eminent energy sources. Energy production due to fossil fuels was a primary contributor to the rise in atmospheric carbon dioxide concentration from 360ppm to 400ppm between 1995 and 2015.[1] Furthermore, because of the large potential for electrification in many developing countries, there is no indication that energy consumption will decrease in the near future. Over 10% of the world's population still lives in extreme poverty and disconnected from grid energy, and the world's population is expected to increase to nearly 10 billion by mid-century.[1] The world will depend more on solar and wind energy to support continued global development while mitigating environmental degradation, but the transience of these renewables hurts their reliability as the possible dominant energy source. One major way to account for this unreliability is by improving energy storage for use during low-output periods.

Vanadium redox flow batteries (VRFBs) are seen as a promising renewable energy storage solution due to their nearly unlimited storage capacity, hindered only by the size of the tank that holds their electrolyte solution. Additionally, they can be left discharged for long periods, and accidental mixing of anolyte and catholyte causes no permanent contamination nor reduction of charge capacity. However, the high cost of the battery's ion-exchange membrane, DuPont's Nafion, restricts the battery's economic viability for widespread installation. Nafion also exhibits high vanadium permeability over time, which severely hinders battery lifespan.[2,3]

Over the last 15 years, many alternative flow battery membrane materials have been researched to address Nafion's flaws. Improved vanadium ion selectivity has been exhibited recently in copolymers and composites containing sulfonated polybenzimidazole (SPBI), sulfonated polyetheretherketone (SPEEK), and polyethersulfone (PES).[2,3] More common polyelectrolytes, such as polystyrene, can be sulfonated to show similar ion exchange properties. In the late 1990's and early 2000's, there was some success using poly(styrene sulfonate) (PSS) as the primary ion-exchange material when grafted onto poly(vinylidene fluoride) or W.R. Grace's Deramic.[2] While these materials showed excellent chemical stability and vanadium ion selectivity, they were limited by low proton conductivity.

Studies show that Nafion conducts protons well because of the natural 4 nm sulfonate ion channels it forms, but these channels might also be large enough for vanadium ions.[2,3] Therefore, orienting the sulfonates on smaller, cheaper polyelectrolytes into similar ion channels while shrinking the channel size might dramatically improve proton conductivity. Inorganic one-dimensional nanomaterials, such as ZnO, TiO_2, and WO_3, are prime candidates to template channels in membranes. These materials are able to form nanowires with diameters down to 10 nm.[4] To this end, it was hypothesized that, when cast with inorganic nanowires, polyelectrolyte sulfonate groups would order themselves around the nanowires, attracted to the Zn^{2+}, Ti^{4+}, or W^{6+} in the crystal lattice. ZnO was predicted to then readily dissolve out of the polymers, leaving behind sulfonate-rich ion channels throughout the membrane. On the other hand, TiO_2 and WO_3 would most likely remain bonded within the polyelectrolytes, thereby orienting charged channels while simultaneously plugging most of their volume. This might inhibit vanadium while enabling the movement of protons.[6,7] The difference in vanadium permeability and proton conductivity between open and plugged ion channels may further elucidate vanadium's mode of

movement through membranes. The polyelectrolyte used was PSS due to its widespread availability and cost-effective fabrication compared to other materials.[8] The aims were as follows:

1. Homogeneously incorporate nanowires into PSS
    a. Confirm PSS sulfonate group electrostatic alignment around nanowires
    b. Enhance membrane chemical and mechanical stability, especially in sulfuric acid solutions
2. Build a battery prototype and study the membrane's long term voltage and coulombic efficiency through charge-discharge cycling
    a. Study battery load response with respect to simulated residential and industrial loads
    b. Study battery charge response with respect to current renewable energy charge behaviors

2. Background and Significance

2.1 Current Energy Landscape: Environmental and Economic Implications

The global energy industry is currently facing widespread changes in technological direction. Data supporting the impact of the energy industry's pollution on the environmental has become widely available with current communication structures. Advocacy groups, citing these claims, are growing in popularity. Energy production due to fossil fuels was a primary contributor to the rise in atmospheric carbon dioxide concentration from 360ppm to 400ppm between 1995 and 2015.[1] Also, the global average temperature has risen by over two degrees Fahrenheit since 1880 (Figure 1). Since these two metric have followed the same trend for the past century, it is widely believed that pollutants released from fossil fuel power plants, such as carbon dioxide, sulfur dioxide, nitrogen oxides, and particulates like carbon black, are a main cause of global warming. They also contribute to other environmental concerns, such as rainwater acidification.

Global warming has been linked to an increased prevalence in extreme weather patterns. Hurricane and droughts are increasing in prevalence and severity, unevenly impairing infrastructure and agricultural productivity in developing equatorial nations compared to developed temperate nations. Furthermore, because of the large potential for electrification in many developing countries, there is no indication that energy consumption will decrease in the near future. Over 10% of the world's population still lives in extreme poverty, and the world's population is expected to increase to nearly 10 billion by mid-century.[1]

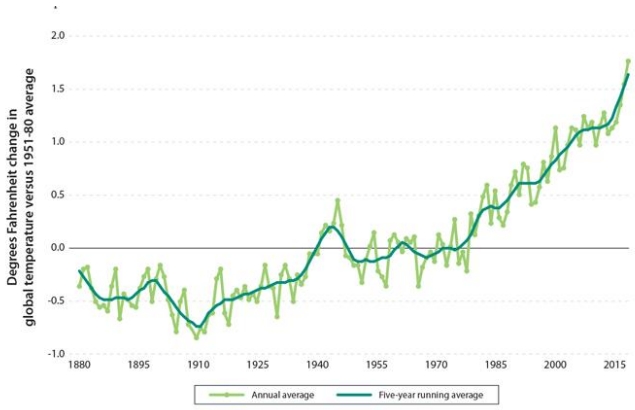

Figure 1. Global Temperature Change Data[33]

Consequently, countries around the world, including the United States, are taking action. There are currently widespread government tax incentives to scale up renewable energy industrially and residentially.[9] The Environmental Protection Agency, through the Clean Power Plan, has released emission standards that aim to reduce carbon dioxide emissions by 32 percent by 2030, subject to review under executive order.[10] Government incentives, combined with increased pressure on fossil fuel standards, has created an economic boom within the renewables industry. Predictions estimate that the renewables will produce over a quarter of the United States' energy by 2050 (Figure 2). In that same time span, solar and wind power combined are predicted to provide over 70% of total renewable energy production.

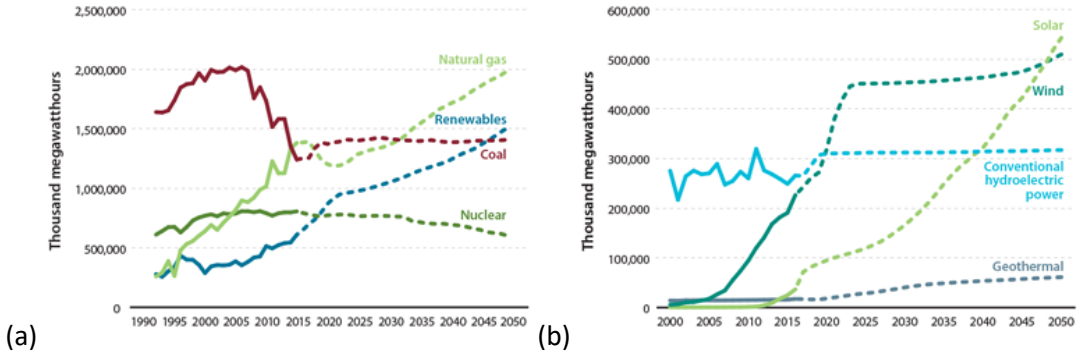

Figure 2. U.S. energy outlook by 2050 (a) predictions for natural gas, renewables, coal, and nuclear (b) predictions for solar, wind, hydroelectric, and geothermal[33]

The continued expansion of renewable energy infrastructure into a dominant position in the energy economy is currently met with a few critical challenges. Primarily, solar and wind energy are both transient sources, highly dependent on weather patterns and time of year. A study in New York found that, at certain hours of the week, the sum total of New York's wind energy production exceeded load demands, while wind energy plummeted at other hours (Figure 3).[11] Similarly, average U.S. insolation from 1960-2005 varied unpredictably by day and cyclically by year in the southwest, the region with the most consistent sunlight predicted to lead the solar infrastructure escalation (Figure 4).[12] Furthermore, solar output is zero at night. This is a problem because it adds a second level of grid uncertainty. In addition to load fluctuation over time, most loads, especially those in urban areas, require a constant baseline amount of power. Therefore, the grid must supply the baseline power and be ready to supply a certain peak level of power at any possible time. This can't currently be satisfied by renewables alone in high-consumption locations.

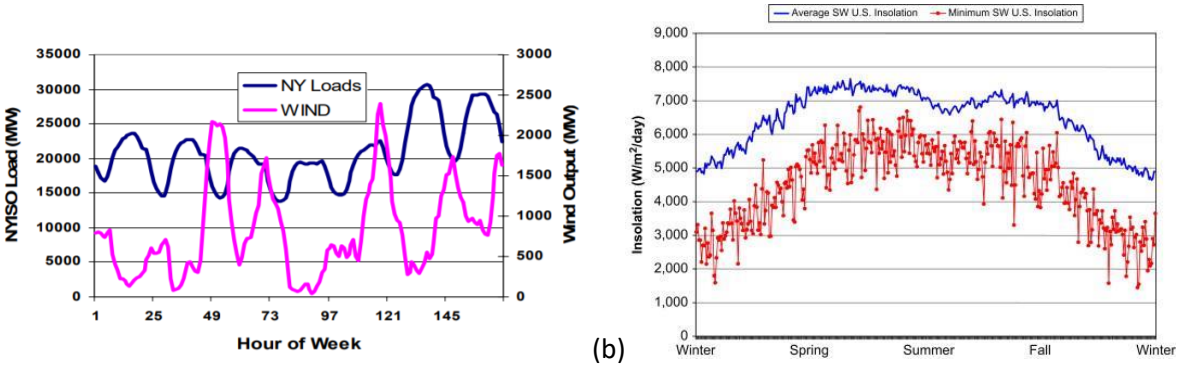

(a) (b)

Figure 3. (a) Hourly Transience of Wind Power in New York[11] (b) Daily and Yearly Transience of Insolation in the American Southwest[12]

2.2 Vanadium Redox Flow Batteries: Structure, Use, and Challenges

One approach to address the unreliability of solar and wind energy is by improving energy storage for use during low-output periods. Vanadium redox flow batteries (VRFBs) are seen as a promising candidate for this application. VRFB's are comprised of an anolyte and catholyte tank, anode and cathode, two pumps, and a proton exchange membrane (Figure 4). During discharging, electrons flow from the load to the cathode and into the catholyte solution, where Vanadium (V) Oxide (VO_2^+) is reduced to Vanadium (IV) Oxide (VO^{2+}). In this case, one oxygen ion is released, which joins with two protons to form water.

In the anolyte solution, Vanadium (II) is oxidized to Vanadium (III). During charging, electrons flow from the charger to the anode and into the anolyte solution, where Vanadium (II) is reduced to Vanadium (III). In the catholyte solution, Vanadium (IV) Oxide (VO^{2+}) is oxidized to Vanadium (V) Oxide (VO_2^+). In this case, water is split to supply the oxygen anions, leaving behind two protons. Regardless of the direction of charge flow, electrolyte fluid is pumped in one direction.

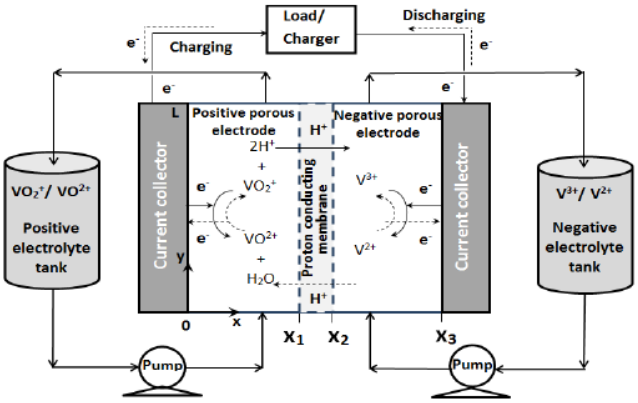

Figure 4. Vanadium Redox Flow Battery Diagram[13]

In this battery configuration, the anolyte and catholyte solutions are each referred to as half cells. As protons are bonded and released during charges and discharges, the proton exchange membrane, located between the half cells, moves additional protons from the electron donating half cell to the

electron receiving half cell in order to equalize electrostatic potential between them. The overall reaction is shown in Figure 5.

$$VO_2^+ + 2H^+ + e^- \rightleftarrows VO^{2+} + H_2O \quad \text{catholyte}$$

$$V^{2+} \rightleftarrows V^{3+} + e^- \quad \text{anolyte}$$

$$V^{2+} + VO_2^+ + 2H^+ \rightleftarrows VO^{2+} + V^{3+} + H_2O \quad \text{overall}$$

(a)

(b)

Reduction reaction	Oxidation state	Colour	Reduction potential (V vs SHE)
$V^{2+} + 2e^- \rightarrow V(s)$	2+	Violet	- 1.13
$V^{3+} + e^- \rightarrow V^{2+}$	3+	Green	- 0.26
$VO^{2+} + e^- + 2H^+ \rightarrow V^{3+} + H_2O$	4+	Blue	0.34
$VO_2^+ + 2H^+ + e^- \rightarrow VO^{2+} + H_2O$	5+	Yellow	1.00

Figure 5. Reactions within vanadium redox flow battery (a) anolyte and catholyte summary (b) properties of aqueous vanadium ions

The difference in chemical potential between vanadium's chemical states on either side of the battery determines the electromotive force (emf or voltage) generated. The voltage developed is specific to the chemical species involved in the reactions and the number and size of cells that are connected in series. In the case of the VRFB, the voltage developed for one stack of cells is generally around 1.41 volts. The current developed by the battery is determined by the number of molecules of vanadium that react within the cells as a function of time. The power delivered is the product of the total current and total voltage developed in the electrochemical cells. The amount of energy stored in the VRFB is determined by the total amount of vanadium available in the volume of electrolyte solution present in the system.[17]

VRFBs are seen as a promising candidate for many reasons. The separation of power and energy is a key distinction compared to other electrochemical storage systems. As described above, the system energy is stored in the volume of electrolyte, which can easily and economically be in the range of kilowatt-hours to 10's of megawatt-hours, depending on the size of the storage tanks. The power capability of the system is determined by the size and number of the stack of electrochemical cells (Figure 6). Unlike solid state batteries, flow battery energy storage elements and charge conversion elements are separated, allowing for energy capacity, voltage, and power to all be tailored independently to grid specifications.[17] They have nearly unlimited storage capacity, hindered only by the size of the electrolyte tanks. They can be left discharged for long periods with minimal self-discharge due to a single state of charge between the two electrolytes. Accidental mixing of anolyte and catholyte causes no permanent damage because the charge carrier is vanadium on both sides.[2] These properties make them ideally suited for large power storage applications. Their limited self-discharge characteristic makes them especially useful for transient renewable energy like solar and wind, where batteries must be able to handle long periods at any level of charge, with little maintenance or supervision. Since it is difficult to predict how much power wind or solar will output in a certain day, this battery's storage versatility can average out production of such energy sources for a grid.

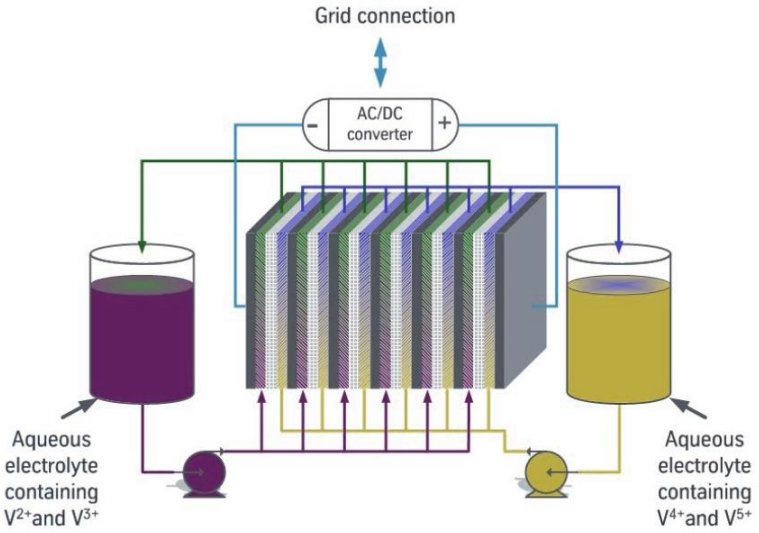

Figure 6. Half Cell Series Connection for Power Scale Up[2] (Note that this does not scale up energy capacity unless fluid is added and tank size is increased.)

On the other hand, their below average energy density requires batteries to occupy a large volume for sufficient storage. This currently restricts their practicality to solely grid energy storage. Most VRFB's in industry operate at an energy density of around 20 Wh/kg of electrolyte, but recent research suggests that the use of precipitation inhibitors along with higher vanadium concentrations can increase this to about 35 Wh/kg[6]. Regardless, this is still much lower than that of lithium-ion batteries, which operate between 80-200 Wh/kg.

Widespread implementation has proved the usability of this technology. There are numerous companies and organizations involved in funding and developing vanadium redox batteries, including Imergy, Vionx, StorEn Technologies, UniEnergy Technologies, and Ashlawn Energy in the United States; Renewable Energy Dynamics Technology in Ireland; Gildemeister AG in Germany; Cellennium in Thailand; Prudent Energy in China; Sumitomo in Japan; H2, Inc. in South Korea; and redT in Britain. The largest vanadium energy storage unit in the world is the Nishi-Sendai Substation in Japan, and the largest in America is the Escondido Substation. The Nishi-Sendai Substation has an energy storage capacity of 60 MWh, much larger than Escondido's 8 MWh. They are both used to regulate solar power plants.

Even though current battery models are able to support certain grids and prove the feasibility of design scale up, they aren't ready for widespread installation yet. The high cost of the battery's ion-exchange membrane, DuPont's Nafion, restricts the battery's economic viability.[15] Furthermore, Nafion exhibits a relatively high vanadium permeability, which severely hinders the battery's potential lifespan.[2,3] While no permanent damage occurs when vanadium ions cross half cells in isolated incidents, a continued stream over time during charges and discharges will slowly diminish charge capacity by lowering the potential difference between half cells. This is compounded by the fact that vanadium ions from opposite sides of the membrane tend to react with one another when they are leaked, thus lowering the pH and causing the electric potential between the half cells to decline even further. The following is a summary of contamination reactions that occur (Figure 7).[16] The first and second reactions correspond to the case where vanadium ions of the catholyte (V(IV) and V(V)) cross through the ion-exchange membrane and

react with V(II) in the anolyte. A similar case occurs when the vanadium ions of the anolyte (V(II) and V(III)) travel through the membrane and react with V(V) in the catholyte according to the third and fourth reactions.

$$V^{2+} + 2VO_2^+ + 2H^+ \rightarrow 3VO^{2+} + H_2O$$

$$V^{2+} + VO^{2+} + 2H^+ \rightarrow 2V^{3+} + H_2O$$

$$VO_2^+ + V^{3+} \rightarrow 2VO^{2+}$$

$$VO_2^+ + 2V^{2+} + 4H^+ \rightarrow 3V^{3+} + 2H_2O$$

Figure 7. Contamination Reactions[16]

2.3 Ion-Exchange Membranes: Function, Use, and Challenges

Alternate flow battery membrane materials has been a popular area of research in order to address the shortcomings of Nafion. The goal of an ion exchange membrane is to be as proton conductive and impermeable to vanadium ions and water as possible. Since vanadium and water are larger than protons, size exclusion is a possibility that has been explored. It is believed that Nafion exhibits high vanadium permeability because it exhibits poor size exclusion, allowing for two modes of vanadium transport.[2,3] The standard mode of transport involves ions continuously bonding to sulfates through the membrane. This is referred to as the surface transport mechanism. Additionally, within membranes, Nafion fibers self-assemble into water-saturated channels that oscillate between 4 nm and 1 nm across.[18] This is due to microphase separation between the hydrophobic Teflon backbone and hydrophilic sulfonated ends. Since hydrated vanadium ions are around 0.6 nm,[21] the channels are large enough for vanadium oxide and water to travel across the membrane without any chemical or electrostatic interactions. This is referred to as the bulk transport mechanism (Figure 7). A goal for many currently researched membranes is to minimize bulk transport as much as possible, considering its lack of selectivity.

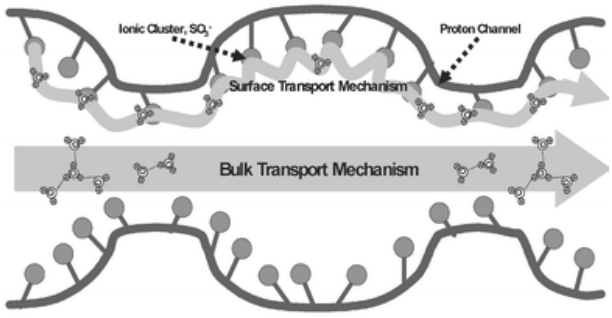

Figure 8. Both surface and bulk transport through Nafion due to 4nm ion channels.[18]

Nafion is extremely expensive because of the process through which it is made. First, a perfluoro (alkyl vinyl ether) with sulfonyl acid fluoride, specifically perfluoro-3,6-dioxa-4-methyl-7-octenesulfonic acid (PFDMOSA), is prepared by the pyrolysis of compounds having the following structures:

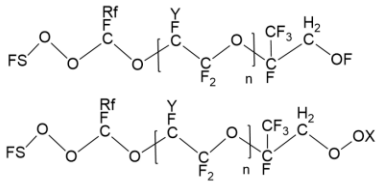

where R_f is a radical that is either fluorine or a perfluoroalkyl radical, Y is a radical that is either fluorine or a trifluoromethyl radical, and n is an integer ranging from 1 to 3. Next, PFDMOSA is copolymerized with tetrafluoroethylene (TFE) (Figure 9). The resulting product is an $-SO_2F-$ containing thermoplastic. Hot aqueous sodium hydroxide converts these sulfonyl fluoride ($-SO_2F$) groups into sulfonate groups ($-SO_3{-}Na^+$). This form of Nafion, referred to as the neutral or salt form, is finally converted to the acid form containing the sulfonic acid ($-SO_3H$) groups.[19] This whole process is much more expensive than the polymerization of newer choices for ion exchange membranes due to the need for two monomers and the large molar mass of the perfluoro (alkyl vinyl ether).

Improved vanadium ion selectivity has been exhibited recently in copolymers and composites containing sulfonated polybenzimidazole (SPBI), sulfonated polyetheretherketone (SPEEK), and polyethersulfone (PES) (Figure 9).[2,3] These polyelectrolytes don't have the long side chains seen on Nafion. In all three cases, sulfur-containing ionic groups are present very close to the polymer backbone. This contributes to smaller ion channel sizes and better size exclusion between protons and vanadium ions. More ubiquitous polyelectrolytes, such as polystyrene, can be sulfonated to show similar ion exchange properties. In the late 1990's and early 2000's, there was some success using PSS as the primary ion-exchange material when grafted onto poly(vinylidene fluoride) or W.R. Grace's Deramic.[2] These materials showed excellent chemical stability and vanadium ion selectivity. On the other hand, the close proximity of sulfates to the polymer backbone diminishes the clear separation of hydrophilic and hydrophobic areas, thus hindering the self assembly of polymer fibers during membrane fabrication and lengthening the mean free path of protons through the membrane. As a result, they are limited by a relatively low proton conductivity.

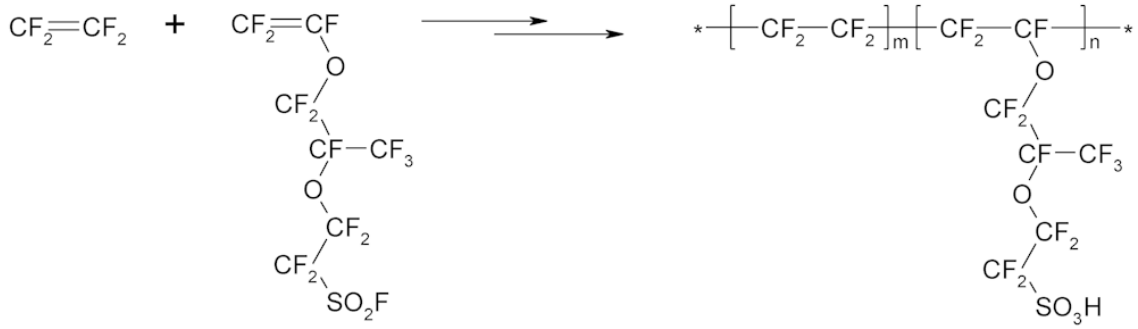

(a)

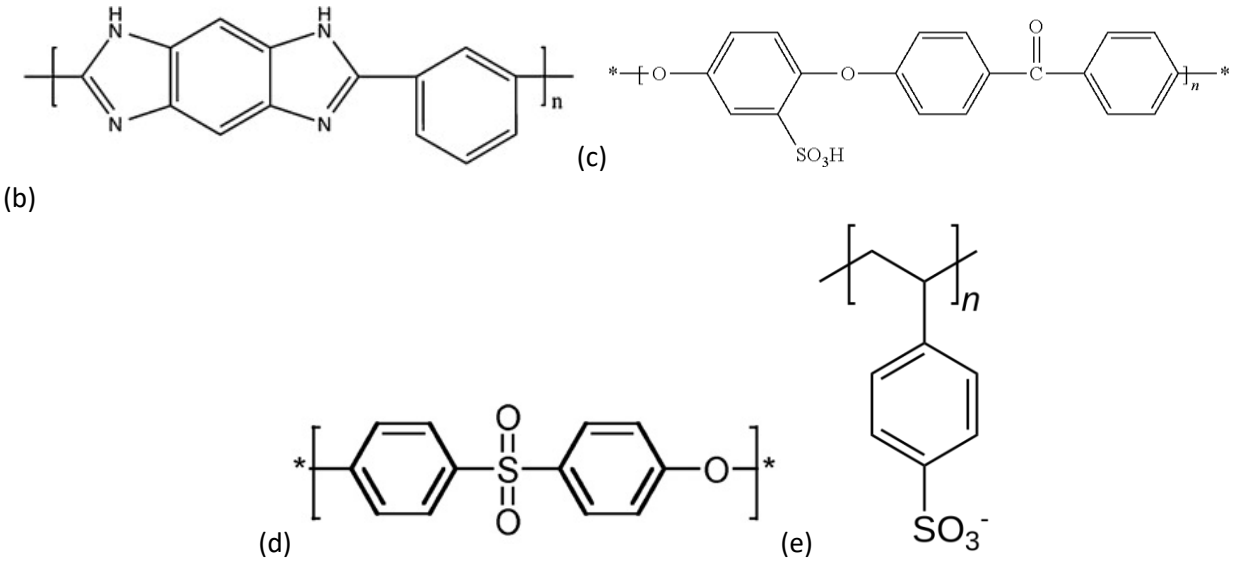

Figure 9. (a)Copolymerization of TFE and PFDMOSA to form Nafion (b) Structure of PBI[21] (c) Structure of SPEEK[5] (d) Structure of PES[22] (e) Structure of PSS[23]

2.4 Inorganic Nanomaterials

Studies show that Nafion conducts protons well because of the natural 4 nm sulfonate ion channels it forms, but these channels are also large enough for vanadium ion bulk transport.[2,3] If there was a way to orient the sulfonates on smaller, cheaper polyelectrolytes into similar ion channels while also shrinking the channel size, proton conductivity would be improved dramatically. Inorganic one-dimensional nanomaterials, such as ZnO, TiO_2, and WO_3, are prime candidates to solve this problem. In this project, it was hypothesized that, when casted with inorganic nanowires, polyelectrolyte sulfonate groups would order themselves around the nanowires, attracted to the Zn^{2+}, Ti^{4+}, or W^{6+} in the crystal lattice and forming ion channels while plugging channel volume. These nanowires are commercially available with diameters between 50 nm and 10 nm.[4] ZnO is soluble in dilute acids, TiO_2 is only soluble in hot concentrated sulfuric acid, and WO_3 is insoluble in acids.

Recent work has shown that SPEEK doped with TiO_2 nanoparticles exhibits improved mechanical stability due to electrostatic interactions between the sulfonate groups and nanoparticles. This membrane also exhibits decreased vanadium ion permeability due to TiO_2 partially plugging the sulfonate ion channels.[5] TiO_2 is also easily functionalized for tailored polymer interactions (Figure 10). For example, sodium hydroxide, triethyl amine (TEA), and 3-aminopropyltriethoxysilane (APTES) have been used to add amine groups in order to not only plug ion channels but improve ion exchange capacity and conductivity.[25] In this case, nanoparticles add ions to the proton transfer route, functioning similarly to the sulfonate groups and adding what literature calls extra “proton hopping sites.” Membranes with 7.5 wt% amine-functionalized TiO_2 showed a 40.8% decrease in swelling, a 132.7% increase in conductivity, and an 86.7% increment in maximum power density. It is possible that moving from particles to wires may straighten channel geometry, furthering the above improvements in transport.

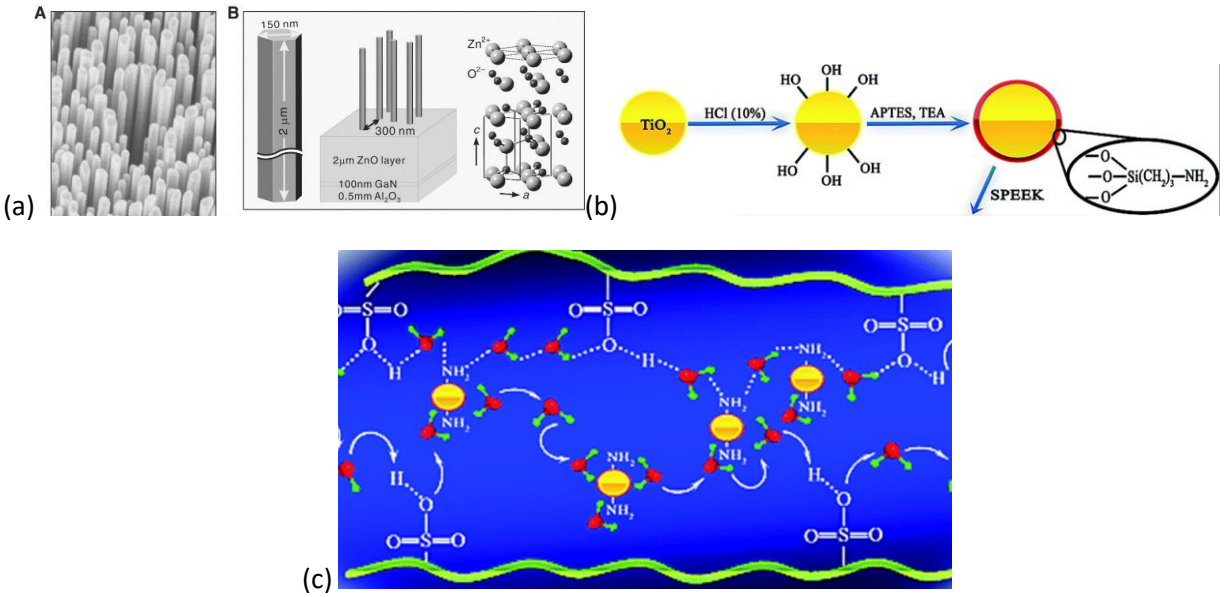

Figure 10. (a) Structure and SEM images of ZnO[24] (b) TiO_2 functionalization with amines[25] (c) Functionalized TiO_2 binding to SPEEK and water for proton transport[25]

Zinc oxide has also found success as an additive in polymer composites. ZnO nanowires and nanoparticles embedded in PES membranes showed improvements in hydrophilicity, water transport resistance, and antifouling. Zinc oxide is also able to be functionalized (Figure 11), having been bonded to 3-hydroxypropanoic acid in order to utilize a hydroxyl end (ZnHM). The hydroxyl group on ZnHM can then be bonded to 2-bromo-2-methylpropionyl (BMP-2) groups (ZnBM). ZnBM, in turn, can be added to both poly(methacrylic acid) (PMMA) and poly(2-(Ncarbazolyl)ethyl methacrylate) (PCEM) in order to chemically link ZnO to these polymers. This may cause better inorganic nanoparticle/polymer conjugate self-assembly compared to separated ZnO and polyelectrolytes self-assembling in solution due to electrostatic interactions alone.

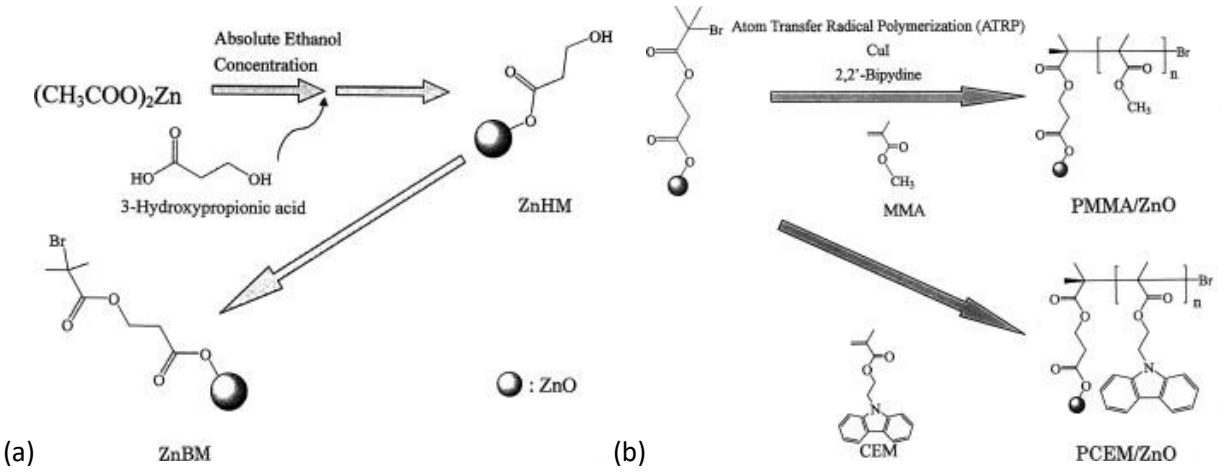

Figure 11. Functionalization of ZnO for fabrication of polymer/ZnO composites[27]

In contrast, WO_3 has not been used for polymer composites nearly to the extent that TiO_2 and ZnO have. However, they have been shown to adhere to hydroxyl groups on methyl cellulose and various polylol dispersing agents, such as ethylene glycol and glycerine. This may point to the possibility of sulfonate groups orienting themselves around WO_3, the largest of the three choice nanomaterials.[28] It's insolubility might be its greatest asset in a flow battery cell that contains either 6M sulfuric acid or 6M sulfate chloride solution, the typical solutions for a VRFB.[7]

2.5 Solar and Wind Grid Loads

As described above, solar and wind energy are projected to be the fastest growing sectors of the energy industry in the near future. In order to gauge VRFB performance when handling loads sustained by these renewables, it is necessary to review load behaviors in which renewables are projected to play a major role. Residential energy is a good model from which to start because it is much more easily monitored in literature.

As mentioned before, residential solar energy is quickly becoming an economically sound choice for homeowners.[9] However, in order to achieve complete energy independence from the grid and operate under full renewable energy, homes will need to be able to account for large spikes in energy use. A study performed on a 1000-home smart grid in Austin, Texas measured electricity use in one-minute intervals for each home for a full year (Figure 12). For an average home, one minute data for ten days, as well as hour averages for the ten days and a monthly average for all of May 2013.[29] Midnight is labeled as hour zero, moving through the day until hour 23, or 11pm. Demand plateaus from midnight to 6 am, when many people wake up and get ready for work. Demand then dramatically rises for a few hours, falls for majority work hours, then spikes again throughout the evening. It is interesting to observe that demand falls during midday when peak solar performance occurs, allowing for batteries to charge.

The biggest takeaway from this data is the suddenness of consumption spikes. The sharpest surges exceed 11 kW within minutes before dropping back down to the average of 3 kW. Fortunately, studies have shown that current VRFB's can achieve a response time of under half a millisecond for a 100% load change and allowed overloads of as much as 400% for 10 seconds.[6]

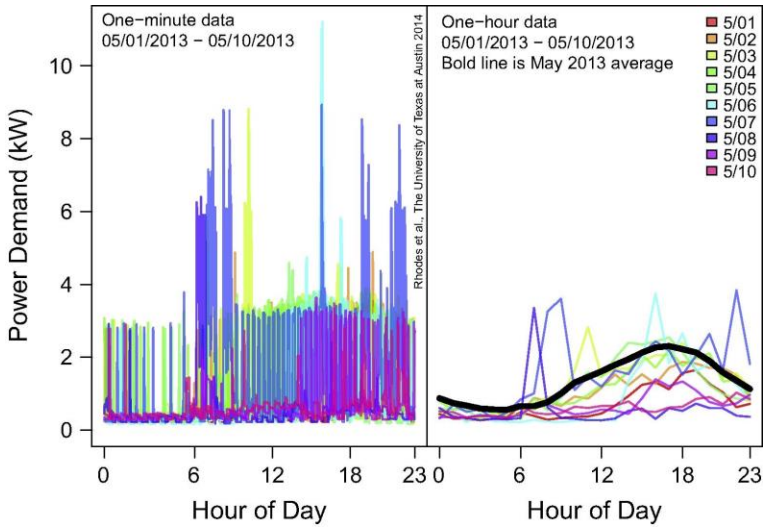

Figure 12. Electrical Power Demand for an Average Austin, TX Home in 2013[29]

It should be noted that residential energy demand is highly dependent on a multitude of factors, such as house model, family size, climate, and season. Studies have shown that summer and winter consumption far exceed spring and fall due to the increased use of heating and cooling systems.[30] The benefit of VRFBs in this regard is their modularity, their ability to have each part tailored to the specific needs of a family. Tank sizes can be scaled in order to supply sufficient energy, while the number and size of alternating half cells in series can be scaled for voltage requirements. Additionally, residential energy demand fluctuations, as a percentage of the capacity of the installation supplying the energy, are much more severe than fluctuations seen on a large scale, especially compared to grids dedicated to industrial consumption. However, diurnal, seasonal, and climatic variations occur in the same manner qualitatively (Figure 13).[30] Since small scales are the most difficult to maintain, the modularity concept applies to scale up for commercial applications with little complication.

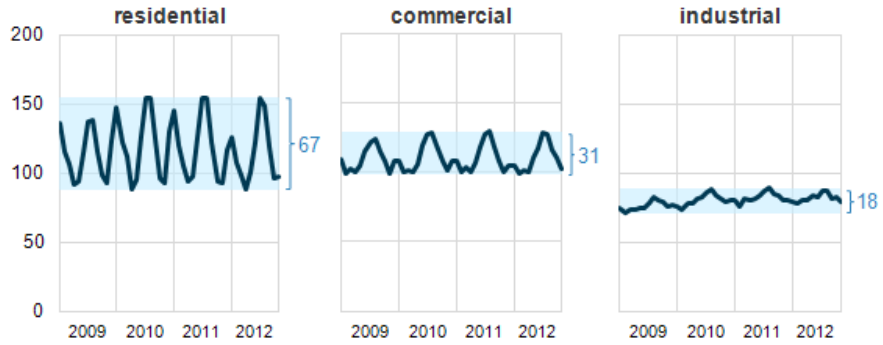

Figure 13. Average Electricity demand by End-Use Sector from 2009 to 2012 (billion kWh)[30]

While current data regarding home energy demand is useful, future projections are more beneficial when designing the performance of cutting edge technology. For example, some projections say that electric vehicle sales will constitute a third of all car sales by 2030.[31] This will completely shift the effect of time of day on residential energy demand. Currently, homes owning electric vehicles charge them throughout the night because of convenience and discounted off-hour electricity, tripling energy use between midnight and 7am compared to typical households (Figure 14).[32] Since solar panels maintain zero output at night, battery size and solar production would need to be increased such that enough energy can be stored during the day for later use. New technologies such as this should be kept in mind when installing residential solar systems that are designed to last for twenty years.

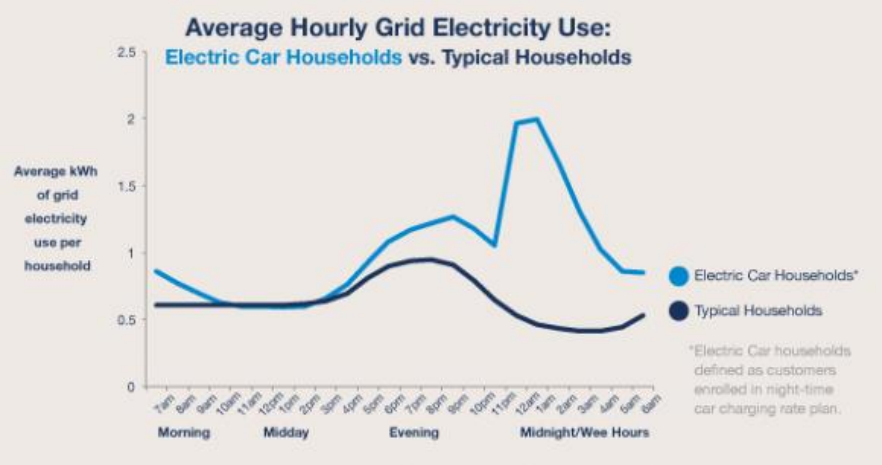

Figure 14. Effect of Electric Vehicle Ownership on Residential Energy Consumption[32]

3. Methodology

3.1 Materials

Zinc oxide nanowires (ZnO, pure powder), poly(sodium 4-styrenesulfonate) (PSS, Mw 200,000, 30 wt % in water), poly(4-styrenesulfonic acid-co-maleic acid) (PSS-MA, Mw 20,000, 25 wt % in water), poly(allylamine hydrochloride) (PAH, Mw 17,500, pure powder), sulfuric acid (95.0 - 98.0%), glutaraldehyde (GA, 25 wt % in water), hydroquinone (ReagentPlus® ≥99.5% powder), divinylbenzene (DVB, technical grade 80%), Vanadium(IV) oxide sulfate hydrate (V^{4+}, 97%), and 4-4'-methylenebis(cyclo-hexykamine) (MBCA, technical grade 95%) were all obtained from Sigma-Aldrich. Glycerol (99+%) was obtained from Alfa Aesar. N,N'-dicyclohexylcarbodiimide (DCC, 99%) and tetraethylenepentamine (TEPA, ≥95.0%) were obtained from Acros Organics. A solid membrane of Nafion-N117 (Chemours brand) was obtained from Fuel Cell Earth. Carbon felt (AVCarb G100 brand) was obtained from Fuel Cell Store. Quarter-inch thick ultra fine grain conductive graphite plates (9015K81) were obtained from McMaster-Carr. A UV lamp (G15T8, λ = 255 nm, power = 15 W) was obtained from Sankyo Denki.

3.2 Dynamic Light Scattering and Scanning Electron Microscopy

For usable polyelectrolyte-nanowire composites to be fabricated, it is primarily necessary to confirm polymer electrostatic adhesion to nanowires. Particle size can be determined by measuring the random changes in the intensity of light scattered from particles in a solution of PSS and ZnO nanowires.[48] This technique is commonly known as dynamic light scattering (DLS), but it is also called photon correlation spectroscopy (PCS) and quasi-elastic light scattering (QELS). Small particles in suspension undergo random thermal motion known as Brownian motion. This random motion is modeled by the Stokes-Einstein equation, which depends on particle size (Figure 15). For this project, a clear increase in particle size means that either nanowires are aggregating on its own or PSS is electrostatically adsorbing to nanowires.

To confirm that the latter option is occuring, zeta potential measurements must also be done. Zeta potential is the electrical potential at a distance away from a charged particle called the slipping plane (Figure 15). In a solution of charged particles, an interfacial double layer of oppositely charged ions may form around the particles. The first layer, or Stern layer, contains anchored oppositely charged ions, and

the second layer, or diffuse layer, contains free flowing ions, albeit more opposite charge than similar charge. The point at which the diffuse layer ends is called the slipping plane. DLS exploits the fact that a charged particle responds to an applied electric field. The frequency of the scattered light is a function of particle velocity due to the Doppler shift, and a change in frequency can be measured upon application of the external electric field.[48] A mathematical model called the Smoluchowski model is then used to calculate zeta potential. It was hypothesized that a clear negative zeta potential would be seen from these measurements, indicating an aggregation of specifically negative charge. This would suggest that the anionic PSS would be electrostatically adsorbing to nanowires instead of the nanowires aggregating separately due to random Brownian motion.

Finally, scanning electron microscopy (SEM) images were also taken to see the evidence of nanowires within casted PSS films. These images were meant to confirm that nanowires were well dispersed within PSS after membrane casting and drying.

$$d_H = \frac{kT}{3\pi\eta D}$$

d_H = hydrodynamic diameter (m)
k = Boltzmann constant (J/K=kg-m2/s2-K)
T = temperature (K)
η = solvent viscosity (kg/m-s)
D = diffusion coefficient (m^2/s)

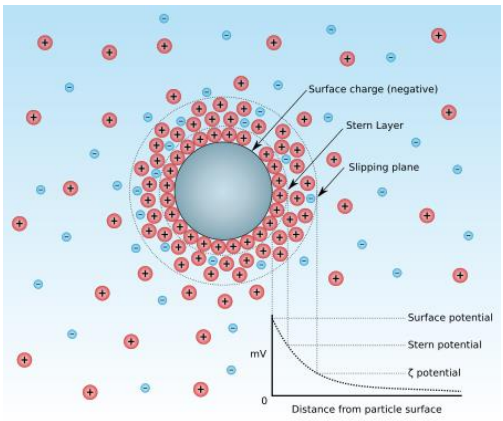

Figure 15. Stokes-Einstein Equation and Zeta Potential[49]

3.3 Dynamic Mechanical Analysis

Dynamic mechanical analysis (DMA) is used to analyze the thermomechanical properties of materials, including storage and loss modulus, at various temperatures. In this case, the case of tensile DMA, membranes were subjected to sinusoidal tensile stress as temperature changed, and the stress-strain behavior was recorded. It was hypothesized that composite films of PSS and ZnO would exhibit unique mechanical behavior on a macro level compared to pure PSS films, especially at low temperatures. This would be further proof of strong electrostatic interactions between inorganic nanowires and PSS. Thusly, 100 µm films of both types were casted, and DMA was conducted at temperatures ranging from -100°C to 25°C.

3.4 Crosslinking Strategies

Once adhesion was confirmed, PSS needed to undergo partial crosslinking to improve its chemical and mechanical stability in a 4-5M sulfuric acid solution with traces of phosphoric acid and ammonium sulfate, additives being researched for future VRFBs[7]. Preliminary solubility tests show that PSS-nanowire composites are very soluble in water, 5M sulfuric acid solution, and 5M sulfate-chloride solution. However, cross-linked PSS resins are insoluble in these solutions. Literature suggests that PSS can be crosslinked directly using UV light or divinylbenzene.[36,37]

3.4.1 UV Light

Literature suggests that germicidal UV light, at a wavelength of around 255 nm, is able to induce crosslinking in PSS by releasing hydrogen atoms from the polymer backbone, which leaves behind reactive backbone radicals. However, multiple other sites on the polymer radicalize as well with no apparent selectivity (Figure 16).[36] FTIR in literature shows that the crosslinking group on the polymer backbone, shown at around 2800 cm^{-1}, radicalizes and crosslinks sufficiently at an exposure time of about two hours. Longer exposure furthers the crosslinking, but it also furthers separation of the sulfate group as well. Therefore, it is a balancing act between preserving conductivity and inducing crosslinking.

For the experiment, a 15 Watt UV lamp was placed 10 cm away from cast film and left for 24 hours. This process was repeated five times. The cast film must be irradiated in an oxygen-free environment, either under vacuum or pure inert gas such as nitrogen or argon, or else the UV light would induce ozone formation. Ozone is reactive enough to break up PSS and halt crosslinking.[34]

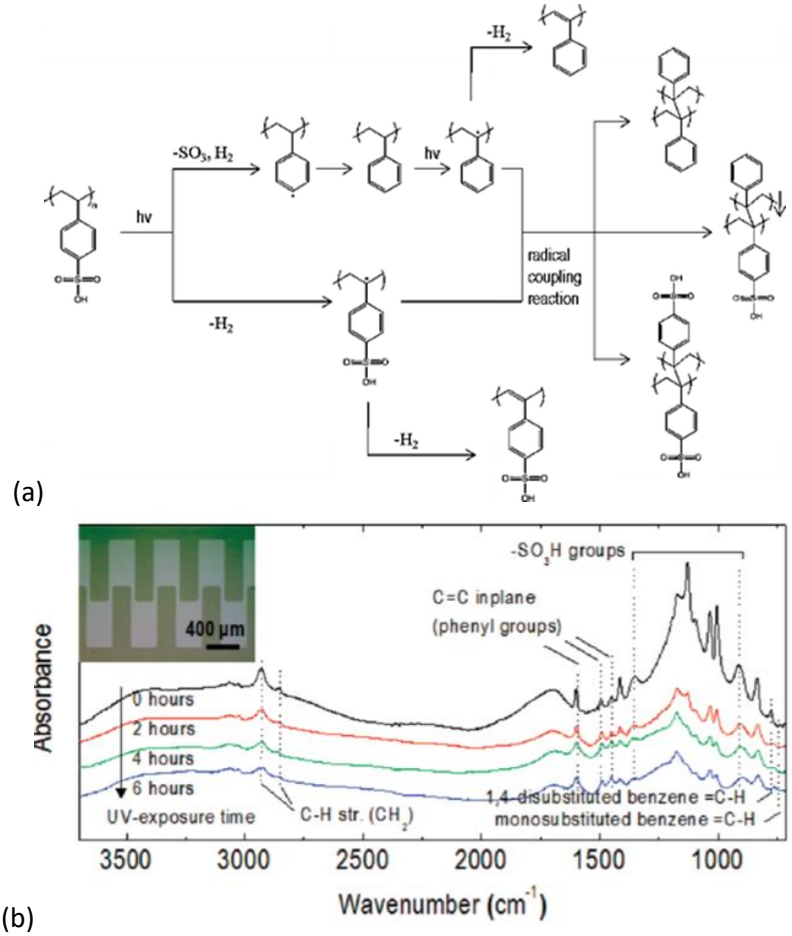

Figure 16. UVC Crosslinking PSS (a) proposed reaction pathways (b) FTIR absorbance spectrum[34]

3.4.2 Divinylbenzene

Divinylbenzene (DVB) is commonly used as a crosslinking agent when one wants to make crosslinked polystyrene from styrene monomers. In this common reaction, DVB and styrene are copolymerized, then the sulfonate group is added to styrene in a second reaction step. This wouldn't work

for our purposes, however, because PSS that is already crosslinked is too rigid to form around nanowires compared to linear PSS. Electrostatic adhesion needs to occur in solution first, then crosslinking must be done on the PSS/ZnO composite afterwards. Therefore, a different option was attempted with DVB. DVB was added to solutions of PSS at a ratio of 1 mol% at 25°C and 65°C in an effort to crosslink across the sulfonate groups themselves (Figure 17). All reactants were added in solution form and mixed with a magnetic stirrer for 12 hours.

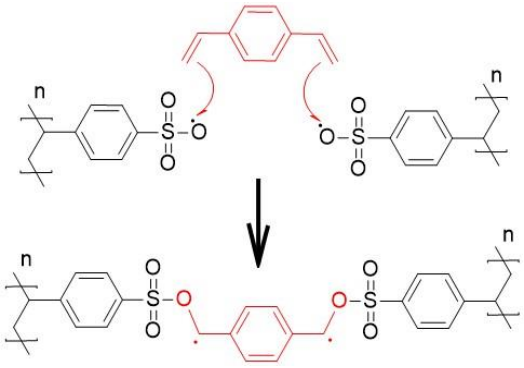

Figure 17. Hypothesized reaction between PSS and DVB

3.4.3 PSS-Maleic Acid Copolymer

3.4.3.1 Hydroquinone Fischer Esterification

Multiple methods of crosslinking a PSS-maleic acid copolymer were attempted. This copolymer was chosen because of the multiple reactions that can be performed on the maleic acid's carboxylic acid group. The first reaction attempted was Fischer esterification with both hydroquinone and glycerol (Figure 18-19). All reactants were added in solution form and mixed with a magnetic stirrer for 12 hours. Two solvents were used, 5M sulfuric acid and 98% sulfuric acid, and reactions were conducted at two temperatures, 25°C and 65°C (Appendix 1).

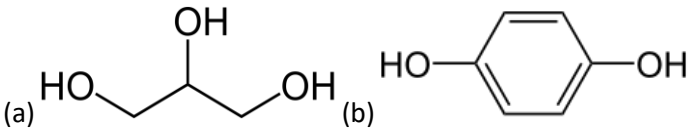

Figure 18. Potential Alcohol Crosslinkers (a) Glycerol (b) Hydroquinone

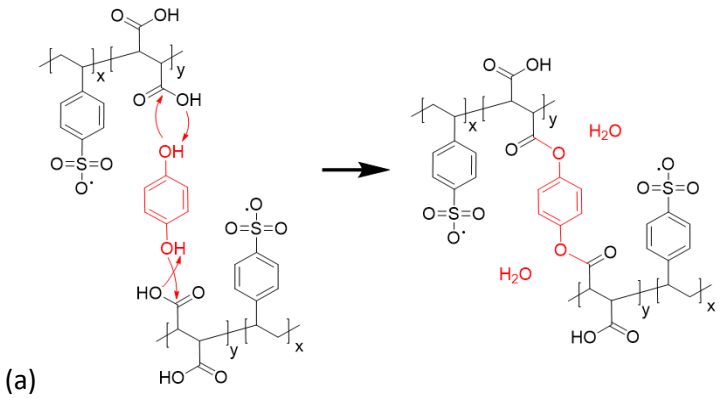

Figure 19. Fischer Esterification (a) Hypothesized reaction scheme between PSS-MA and hydroquinone

3.4.3.2 Amines and DCC

The second maleic acid crosslinking reaction attempted was amination of the carboxylic acid (Figure 20). The direct conversion of a carboxylic acid to an amide is difficult because amines are very basic and tend to convert carboxylic acids to their highly unreactive carboxylate ions. Therefore, dicyclohexylcarbodiimide (DCC) is used to catalyze this reaction. The two crosslinkers attempted as reactants were 4,4'-Methylenebis(cyclohexylamine) (MBCA) and Tetraethylenepentamine (TEPA). All reactants were added in liquid/solution form and mixed with a magnetic stirrer for 12 hours. Two solvents were used, 5M sulfuric acid and 98% sulfuric acid, and reactions were conducted at two temperatures, 25°C and 65°C (Appendix 2).

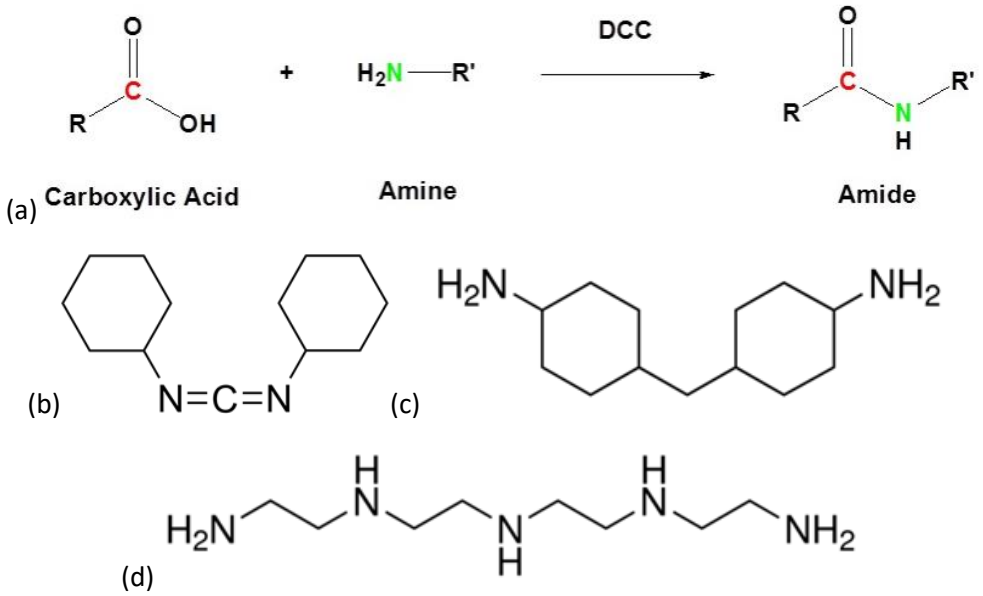

Figure 20. DCC Catalyzed Amination (a) hypothesized reaction scheme[50] (b) DCC: N,N'-Dicyclohexylcarbodiimide (c) MBCA: 4,4'-Methylenebis(cyclohexylamine) (d) TEPA: Tetraethylenepentamine

3.4.4 PSS/PAH Polyelectrolyte Complex and Glutaraldehyde

The final attempted crosslinking method was from an entirely different approach. Two polyelectrolytes were used, the polyanion PSS and the polycation poly allylamine hydrochloride (PAH). These polyelectrolytes usually form complexes (PECs) when combined in aqueous solution, and they also coacervate at high enough ionic strengths. However, this approach was altered slightly by adding liquid glutaraldehyde at various mole percentages. Glutaraldehyde binds rapidly to amines, and it was hypothesized that the glutaraldehyde would crosslink PAH while PAH holds PSS in place (Figure 21).

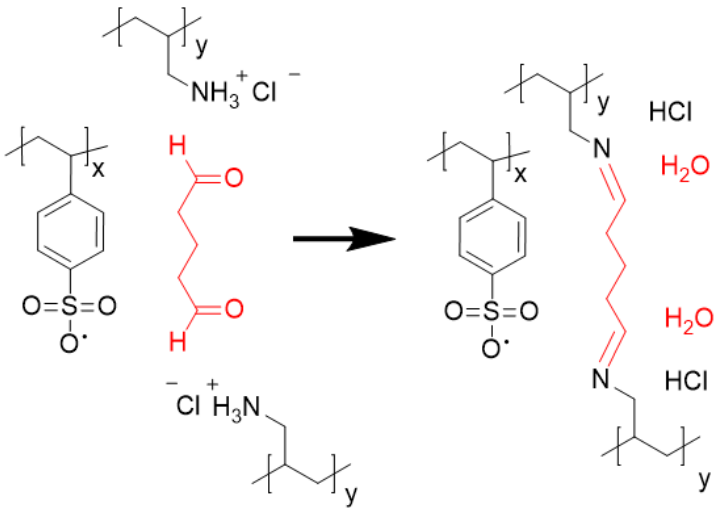

Figure 21. Dehydration reaction scheme

3.5 Battery Prototype Experiments

3.5.1 Battery Assembly and Characterization

In parallel to membrane studies, a battery prototype was designed and built in order to prepare for future membrane charge/discharge performance testing (Figure 30). The prototype battery was built according to the specifications of the inventor of the VRFB, Dr. Maria Skyllas-Kazacos.[2] From center outward, the battery materials are: a Nafion membrane, silicone rubber gaskets, 3D printed acrylonitrile butadiene styrene (ABS) hollow frames that direct the flow of battery solution, carbon felt electrodes that fill the ABS frames, a second pair of silicone rubber gaskets, either copper or graphite current collectors, a third pair of silicone rubber gaskets, and finally an aluminum frame that holds it all together. Silicone tubes attach to the ABS frames, run through peristaltic pumps, and enter flasks holding either the anolyte or catholyte solution. The battery solutions consisted of 0.1M V^{4+} and 5M SO_4.

(a) 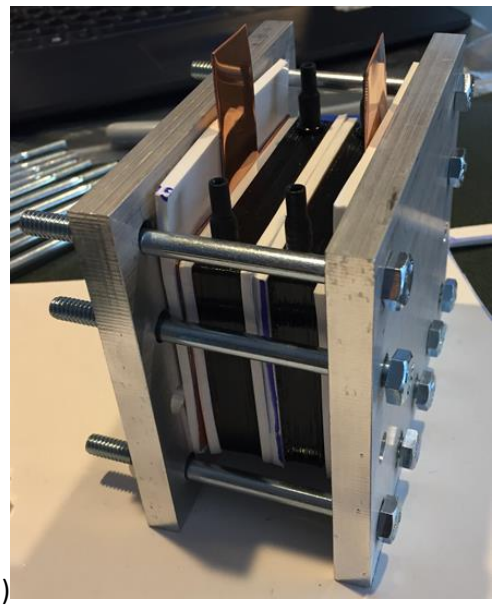

(b) 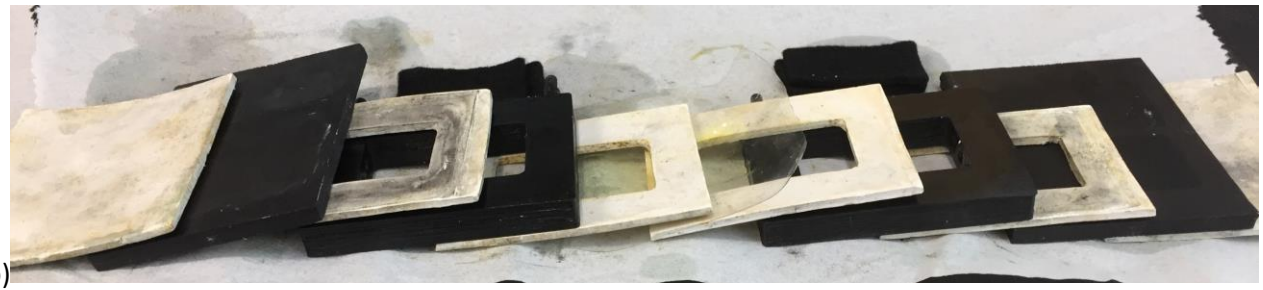

Figure 22. Battery prototype build (a) assembled (b) dismantled to show each layer

3.5.2 Charge Cycling Transient Analysis

According to IEEE Standards, load testing is the only necessary experiment necessary to gauge the performance or health of a battery.[41] Long term load test cycling is the measurement that most accurately models how the membrane would behave in an industrial setting over multiple charge-discharge cycles. During this, the battery is simply charged and discharged over a long period of time, and battery performance is gauged in terms of coulombic, voltage, and energy efficiency. Coulombic efficiency is the ratio of charge current to discharge current multiplied by the ratio of time to charge versus time to discharge. Voltage efficiency is the ratio of voltage decrease during discharging to voltage increase during charging. The energy efficiency is the multiplication of voltage and coulombic efficiencies.[39] The highest energy efficiencies seen are around 90% using PBI membranes.[38]

In order to record battery voltage and current during charges and discharges, an original testing apparatus was built using the Particle Photon, a WiFi-enabled embedded computer (Figure 23). During charges, a 10 Ω resistor was put in series with the voltage source and the battery, and the voltage across this resistor was sent to an anolog input port on the Photon. During discharges, the 10 Ω resistor was used as the sole load for the battery between anode and cathode, and once again, the voltage across it was sent to the Photon. To record the battery's internal resistance, the battery's open circuit voltage was measured immediately before measuring the battery's voltage with the 10 Ω load, and the internal resistance was calculated using the subsequent voltage drop. In order to record and store data from the Photon, a function was written that sent input resistor voltage readings to the online graphing website ThingSpeak via WiFi. This way, battery voltage and current could be monitored in real time from the internet, regardless of the scientist's location. The data was then able to be downloaded and analyzed appropriately.

3.5.3 Corrosion

In order to examine the effects of corrosion, carbon felt battery electrodes were weighed before and after charges. Literature reports that the development of a high cathode potential causes oxidation of the carbon felt with the amount of CO_2 evolution proportional to the cathode potential above 1.0 V. Above 1.2 V, CO is generated electrochemically as well.[50]

(a) 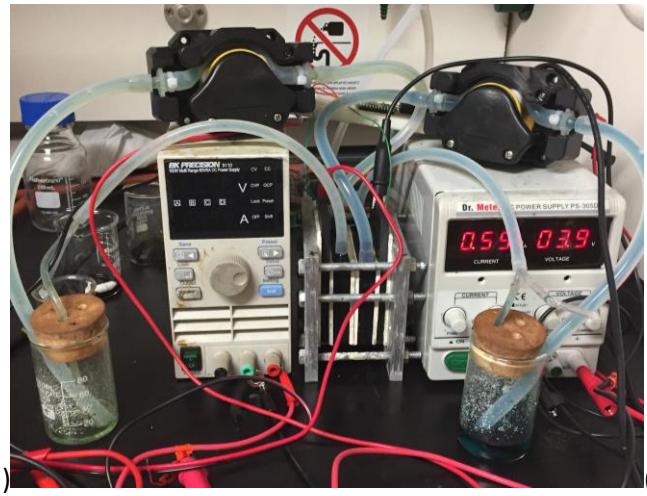

(b) 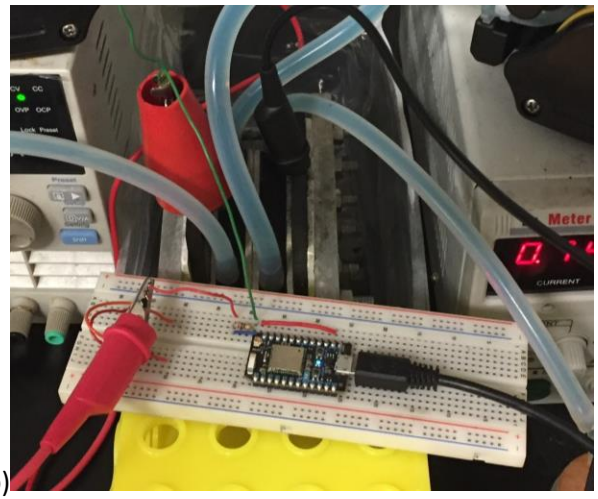

(c)

```
#define publish_delay 20000
unsigned int lastPublish = 0;


void setup() {
}

void loop() {
    unsigned long now = millis();
    if ((now - lastPublish) < publish_delay) {
        return;
    }

    int volt = analogRead(A1);
    float voltage = volt*.8; //voltage reading in mV

    Particle.publish("thingSpeakWrite_A1", "{ \"2\": \"" + String(voltage) + "\", \"k\": \"58GRW2HBGF5IF2M5\" }", 15, PRIVATE);

    lastPublish = now;
}
```

Figure 23. Full battery prototype system (a) solutions, battery, pumps, and voltage sources (b) battery connected to Particle Photon embedded computer for data acquisition (c) Particle code used for data transmission to online graphing software ThingSpeak

4. Results and Discussion

4.1 Dynamic Light Scattering

During DLS size measurements, particle size increases confirmed general aggregation of polymer onto nanomaterial (Figure 24). The ZnO control solutions seemed to measure a mean particle size of 411 ± 103 nm, while combined solutions measured a mean of 445 ± 103 nm, regardless of adsorption time after five minutes. This suggests that aggregation is relatively fast and consistent. Since purchased ZnO nanowires were specified to have a length of 300 nm, DLS measurements seem to be measuring within one and two nanowire lengths, showing some control aggregation which contributes to the wide standard deviation.

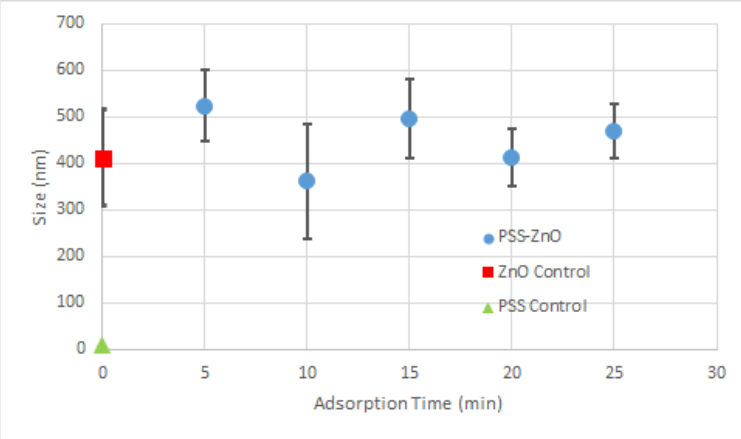

Figure 24. Size Measurements vs Adsorption Time are Relatively Constant

Furthermore, zeta potential was measured at -23 ± 11 mV for ZnO control and -40 ± 6 mV for PSS control, but it rose to -67 mV for combined solutions (Figure 25). The PSS used was in sodium salt form, meaning that every sulfate anion had a corresponding sodium cation in solution. The Zeta potential increase suggests that PSS is not only adsorbing to ZnO due to random aggregation but is preferentially adsorbing compared to the positively charged sodium ions. It was hypothesized that this indicates electrostatic attraction. Furthermore, conductivity measurements in mixed solutions show erratic, high conductivity immediately after mixing, but conductivity drops to about 0.7 mS/cm consistently for any further absorption time. This may be further indication that the PSS sulfate groups are free for conduction in solution before adsorption, but electrostatic bonding between Zinc cations and sulfate anions may prevent electrons from moving during conduction tests.

(a)

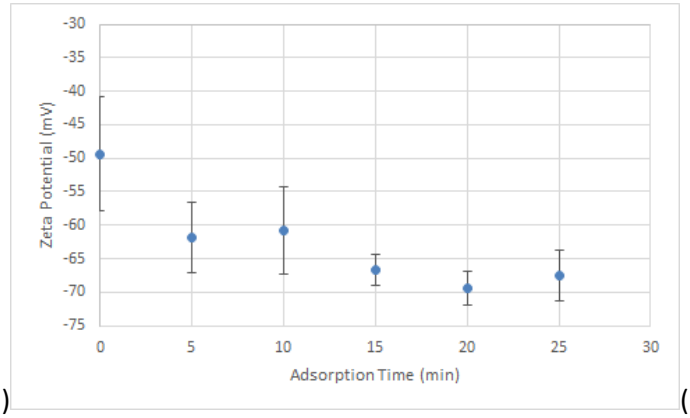

(b)

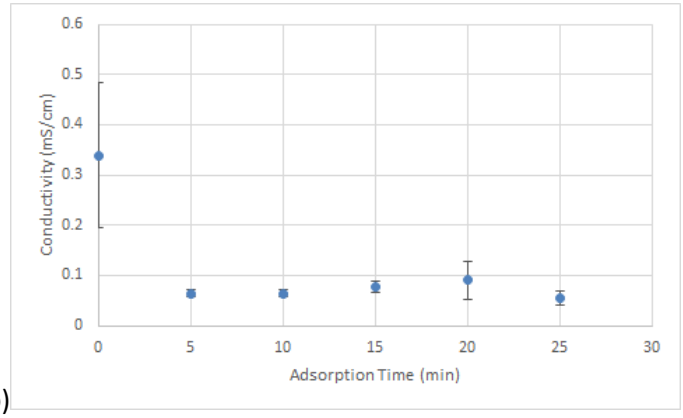

Figure 25. DLS Zeta Potential Data (a) Zeta Potential vs PSS adsorption time on ZnO (b) Conductivity vs PSS adsorption time on ZnO

Finally, SEM images on membrane edges confirm that nanowires are dispersed relatively evenly in PSS membranes (Figure 26). In these images, the rod-like outcroppings on the edges are nanowires. Their presence gives the membrane edges a highly jagged morphology.

(a)

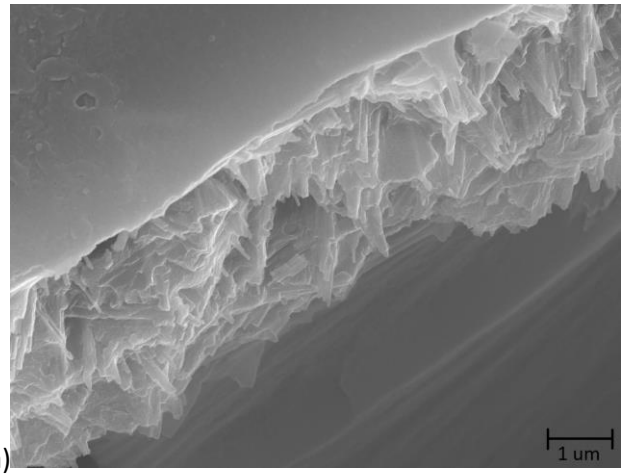

(b)

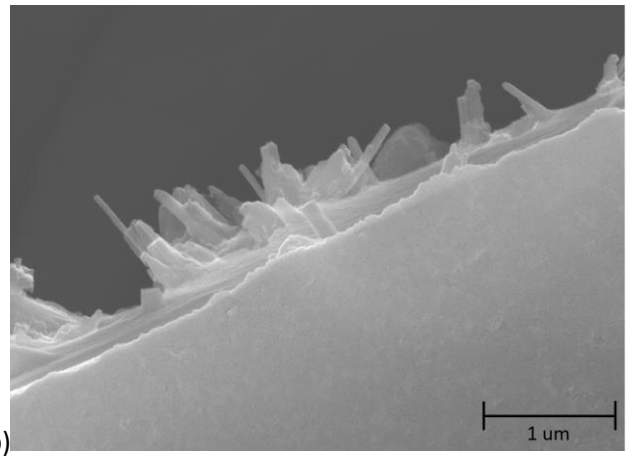

Figure 26. SEM images of nanowires embedded within PSS films

4.2 Dynamic Mechanical Analysis and Scanning Electron Microscopy

It was hypothesized that DMA would show a higher tensile storage modulus and glass transition temperature, similar to the effect of rebar in concrete, for composite membranes at temperatures below -50°C. In contrast, the resulting curves show that, at least for now, composite films show no clear trend of differing from the mechanical properties of pure PSS films (Figure 27). Though the data for composite films was pretty consistent, some pure films displayed higher storage modulus and tan delta than composite PSS, and some show lower metrics. It is possible that these discrepancies are due to slight differences in film thickness or casting dispersion. However, more DMA must certainly be done in the future to confirm these preliminary measurements.

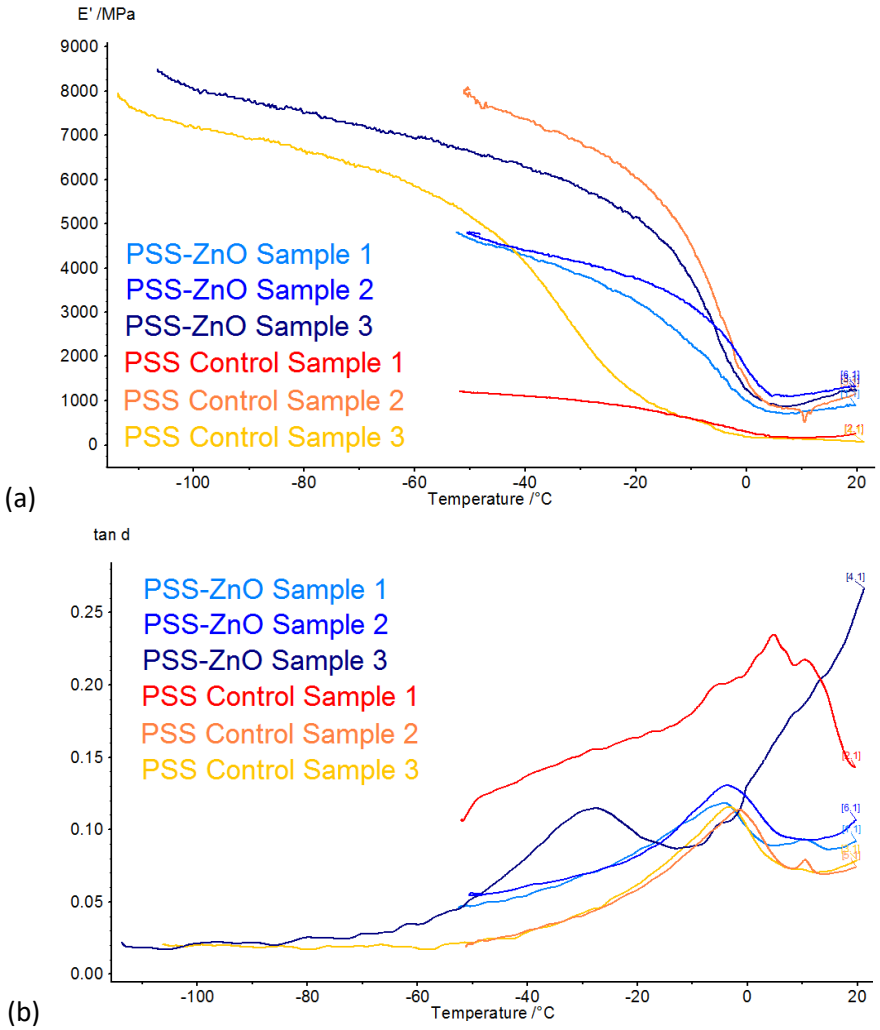

Figure 27. DMA measurements versus temperature (a) storage modulus (b) tan delta

4.3 Crosslinking Strategies

4.3.1 UV Light

Samples irradiated with UV light did not crosslink sufficiently. Each sample fully dissolved in water a day after UV exposure. The main hypothesis for this behavior is that the UV light did not fully penetrate the films, which were 100 um thick. Most literature has only dealt with spin-coated thin films at a thickness of 300 nm.[34] A higher wattage UV lamp may create better results, but if not, then this method should probably be reserved strictly for very thin films.

4.3.2 Divinylbenzene

DVB also did not crosslink membranes sufficiently, as casted films made from this solution fully dissolved in water. It is hypothesized that the oxygen anion in the sulfonate is stable enough to not react with the double bonds of DVB. This option was the least desirable regardless, since successful crosslinking would also mean the inactivation of sulfonate ions in the proton transport chain.

4.3.3 PSS-Maleic Acid Copolymer

4.3.3.1 Hydroquinone Fischer Esterification

These reactions consistently didn't create crosslinked membranes as well. It is hypothesized that this reaction failed because it is equilibrium-driven, and the alcohol groups on both reactants cause the release of water (Figure 23). Since the intended environment of the crosslinked polymer is an aqueous battery solution, the reaction was done both in water and in an actual VRFB battery solution. In both environments, it is hypothesized that outside water molecules drove this equilibrium reaction to the reactant side, based on Le Chatelier's principle. Also, in the case of hydroquinone, another issue is that it tends to self-oxidize to the yellow-brown colored benzoquinone instead of reacting, and a brown color formation was definitely observed in this lab's reactions (Figure 28).

Figure 28. Hydroquinone and PSS-MA post-reaction

4.3.3.2 Amines and DCC

These reactions were also consistently unsuccessful. It is hypothesized that these reactions failed because DCC was unable to catalyze the reaction effectively before the crosslinker's amines converted the carboxylic acids on maleic acid to carboxylates. MBCA crosslinker is bought as a thick, waxy gel that is tough to break apart (Figure 29). Therefore, there might not have been enough crosslinker dissolving into the solution of polymer and DCC for a fully crosslinked resin to be formed. Additionally, both crosslinkers are quite large. DCC must first bind to the carboxylic acid in order for the crosslinkers to conduct a nucleophilic attack on the acid.[50] Since DCC has large aromatic groups as well, there might be too much steric hindrance for nucleophilic attack to be vigorous. Finally, alternative solvents, such as DMF, have proven successful in literature.

Figure 29. PSS-MA, DCC, and MBCA immediately after reaction

4.3.4 PSS/PAH Polyelectrolyte Complex and Glutaraldehyde

Unlike the previous crosslinking experiments, this reaction approach proved to be a relative success. These reactions occurred extremely rapidly, forming gels that absorbed all of the water in the reaction solution in under 5 minutes (Figure 30). At crosslinking densities under 21 mol%, these gels held together very well compared to non-crosslinked complexes, forming little homogenous pucks. At crosslinking densities over 21 mol%, crosslinking was too ubiquitous for complexation to be homogenous, and dense shards would separate from each other once the reactions finished. Most importantly, these complexes were insoluble in water, an essential property of a battery membrane candidate.

While these results were a major step forward in this study, the PEC membranes are not ready yet to be used in a battery for a few reasons. First, the presence or absence of water drastically changes the morphology of these complexes. When hydrated, the complexes were able to be cut with moderate manual force. When dried, the complexes consistently shrank and became extremely hard and strong, but their gel structure could be restored by re-submersion in water. While they are insoluble in water, they do swell and become too soft to clamp into a battery (Figure 31). Increased crosslinking proved to reduce swelling, but it also increased brittleness and tendency to fall apart into dense shards, as reported above. Therefore, for this material to be seen as viable, an ideal crosslinking density needs to be found that preserves homogeneity and reduces swelling.

Secondly, these complexes currently need to be thick membranes in order to hold together strongly, around 5 mm. Nafion, on the other hand, has much higher mechanical strength than crosslinked PSS/PEC complexes, and its thickness is roughly 0.2 mm (Figure 32). The highest performing membranes exhibit increased coulombic efficiency as thickness increases due to decreased vanadium ion permeability, but they also exhibit decreased voltage efficiency as thickness increases due to increased resistance to protons. This creates a thickness balancing act between the two efficiencies to maximize the product of the two, energy efficiency, and ideal thicknesses are around the thickness of the lab's Nafion membranes. Alternative reaction approaches and geometries, wider than the standard 50 mL beakers used for these reactions, must be considered in order to cast thin films in under 3-5 minutes during the reaction process.

Finally, these membranes do not have the ability to handle 2.5 M-5 M sulfuric acid yet. An hour after submersion in battery solutions containing 2 M V^{5+} and 5 M sulfuric acid, the solution turned black (Figure 33). Since sulfuric acid is a powerful dehydrating agent, this usually indicates that the acid has reduced some of the organic material to pure carbon. Perhaps the use of materials with more C-F bonds,

the strongest bond in organic chemistry, will improve chemical stability. Much of Nafion's stability comes from its prevalent C-F bonds.

(a)  (b) 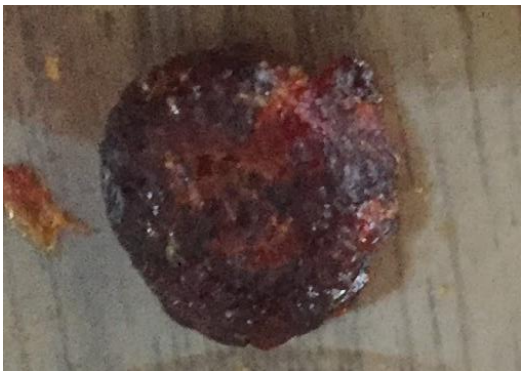

Figure 30. Glutaraldehyde PEC Crosslinking (a) 14 mol% crosslinked membrane immediately after reaction (b) 14 mol% crosslinked membrane left out to dry 24 hrs after reaction

(a) 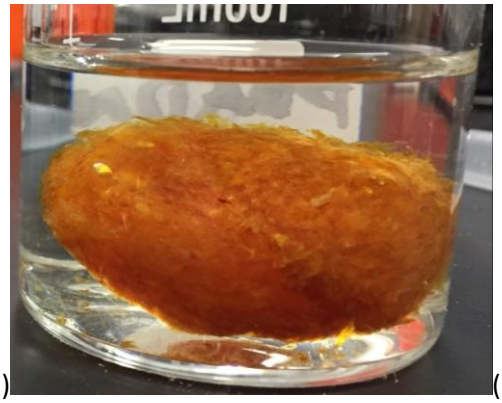 (b) 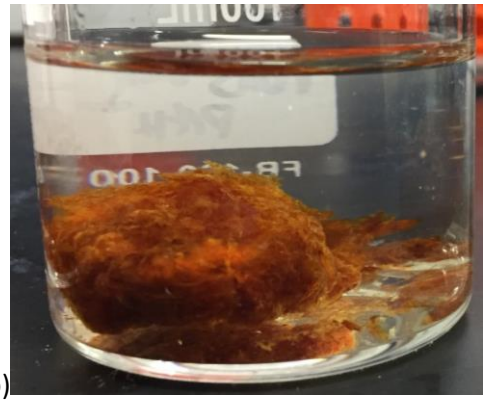

(c) 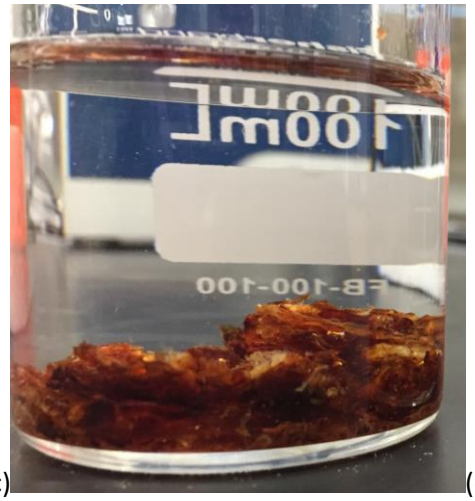 (d) 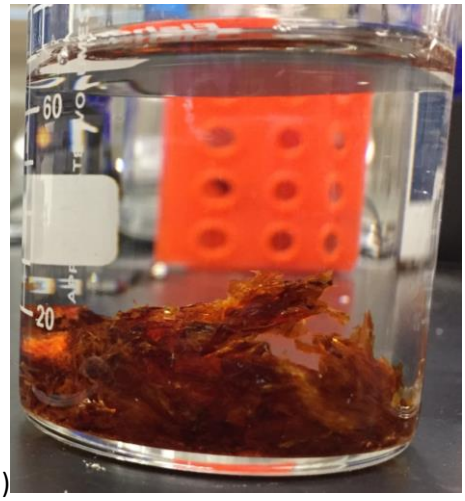

Figure 31. GA crosslinked PSS/PAH swelling. mol% crosslinking: (a) 14% (b) 21% (c) 34% (d) 68%

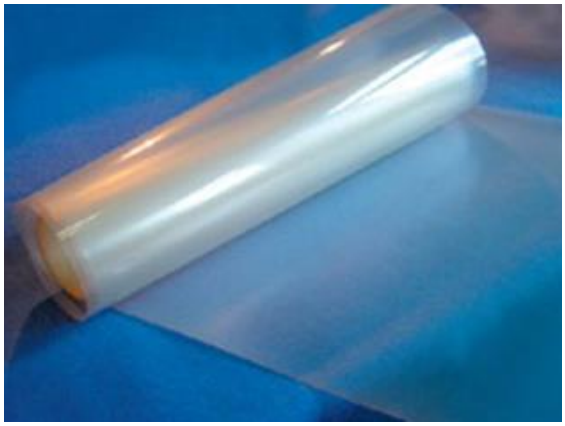

Figure 32. Nafion Film

Figure 33. PSS/MA crosslinked PEC: degradation in 5 M sulfuric acid

4.4 Battery Prototype Experiments

4.4.1 Battery Characterization

In order to prove that the battery was built correctly and performed well, an initial test charge was performed. The voltage source was connected to the copper current collectors and set to 1.8 V. If all goes well, the catholyte would oxidize to yellow V^{5+}, and the anolyte would reduce to green V^{3+}. Very surprisingly, both anolyte and catholyte solutions turned green, indicating that they both reduced. Because of this, a thorough materials analysis was conducted to isolate the materials that could reduce battery solutions on their own. Each material was placed in a flask of battery solution and left for 12 hours.

The copper was the first material to show a green color, reducing pretty easily, and the carbon felt followed a few hours later (Figure 34). Conversely, the silicone rubber gaskets, tubing, and graphite current collectors did not reduce the battery solution. When this was repeated with solutions that contained 2.5 M SO_4, the carbon felt electrodes also did not reduce vanadium. Therefore, the copper was exchanged for the graphite current collectors, and the battery solutions were diluted from 5 M SO_4 to 2.5 M SO_4. The vanadium concentration was kept at 0.1 M. After these modifications, a subsequent test charge successfully reduced the anolyte and oxidized the catholyte. These changes remained for the rest of the study. In order to reduce the anolyte further from green V^{3+} to darker V^{2+}, only the catholyte was exchanged for uncharged V^{4+}, and another charge was conducted. This was the first instance of the lab's successful creation of charged vanadium redox flow battery solutions (Figure 35).

(a) 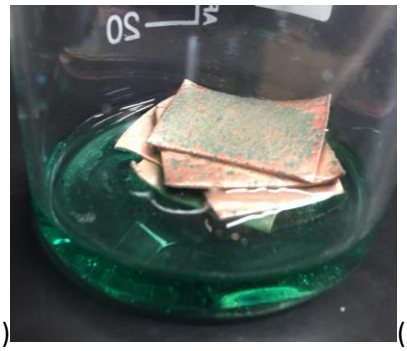 (b) 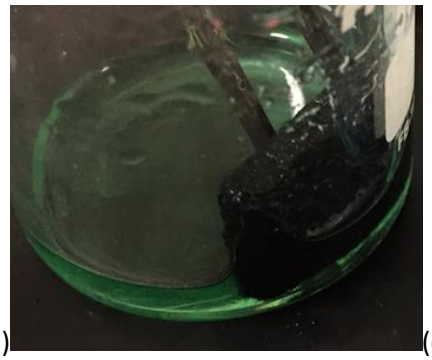 (c) 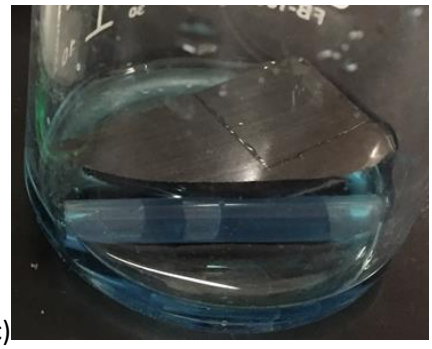

Figure 34. Material reduction in V^{4+} and 5M sulfuric acid (a) copper caused reduction (b) carbon felt caused reduction (c) graphite and silicon rubber tubing did not cause reduction

(a)  (b) 

(c) 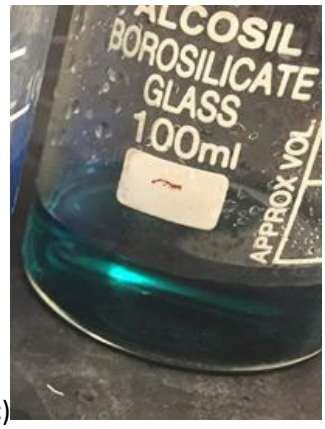

Figure 35. Solutions after complete charge (a) Cathode V^{5+} (b) Pre-charge V^{4+} (c) Anode V^{2+}

4.4.2 Charge Cycling Transient Analysis

Transient analysis results show a mixture of positives and negatives. The positive is that, for only 40 mL of battery solutions at a vanadium concentration 20x lower than industry standards, that battery is able to run for a long time. Current still flows upwards of 14 hours after the beginning of charges and discharges. Current starts relatively high and drops linearly for about 4 hours, then it levels out for the long term (Figure 36). Another positive is the charge and discharge consistency, as exhibited by the data's tight error bars. The negative is the extremely high internal resistance. Based on battery voltage before and after adding a load during multiple charges and discharges, the internal resistance is in the range of 80-150 Ω. This is a massive hindrance to the practicality of this battery. Charging at a voltage of 2.3 V induces a current in the range of 50-80mA, while the discharge current for a 10 Ω load is in the range of 1-8 mA. At 14 hours of lifetime, this means that the battery has a charge capacity of 710 mA-hrs and a discharge capacity of 34 mA-hrs, equating to a coulombic efficiency of roughly 5%. This is miles behind the 93% coulombic efficiency of commercial Nafion-based flow batteries.

One reason for the high internal resistance might be the graphite current collectors. Usually expensive glassy carbon or carbon polymer current collectors, which have much higher conductivity, are used. This might be a prudent investment for future studies. Another likely issue is the battery thickness. The current distance between current collector and Nafion membrane is 3 cm. The mass transfer complications for vanadium ions on this length scale from the membrane, through 4 layers of carbon felt,

to the graphite might play into hindering effective electron movement. An idea for improvement might be 3D printing much thinner frames and using thinner silicone rubber gaskets. Battery prototypes in literature seem to be much thinner than the one used in this set of experiments. Alternative battery geometries in literature may mitigate this issue as well.

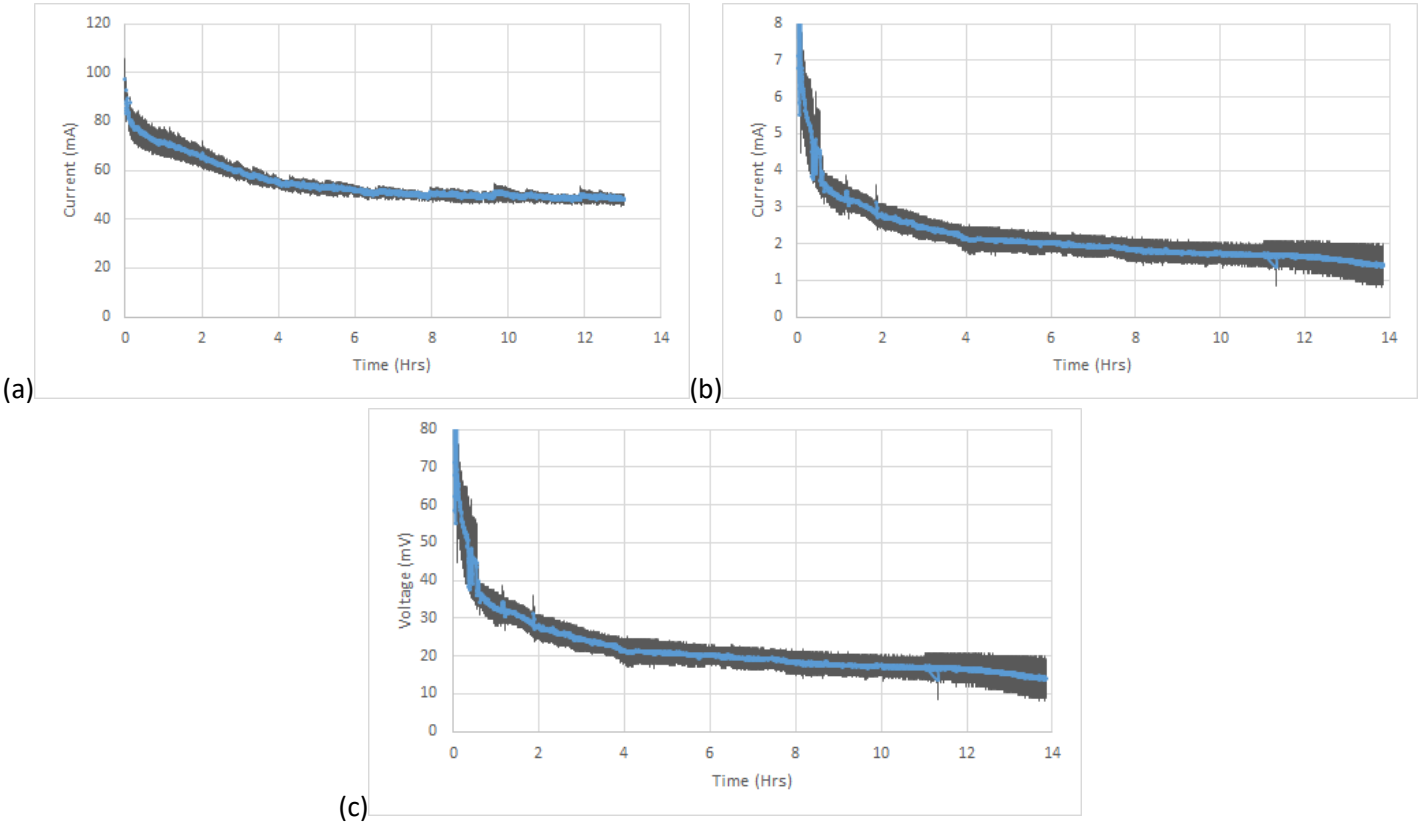

Figure 36. Battery charge transients (a) Charge Current (b) Discharge Current (c) Discharge Voltage

4.4.3 Corrosion

The effect of corrosion after battery use is quite apparent, but only on the cathode side. On this end, carbon felt electrodes routinely lose more than 10% of their weight after 2 complete charge and discharge cycles. This degraded carbon soot appears in the catholyte and on the graphite current collector (Figure 37). This corrosion should be taken into account for future studies when buying ample material for multiple battery experiments. If the same quality carbon felt is bought again, the felt on the cathode side should be replaced after, at the most, 4 to 5 charge discharge cycles.

(a) 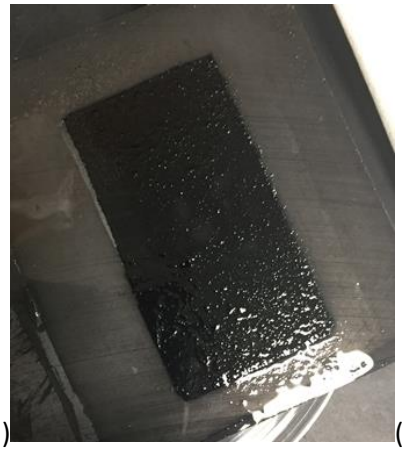 (b) 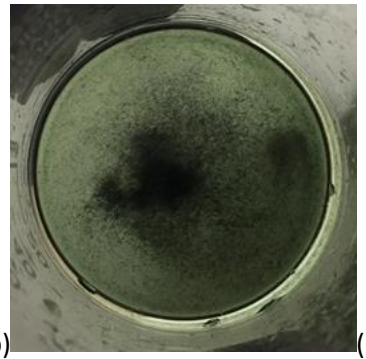 (c) 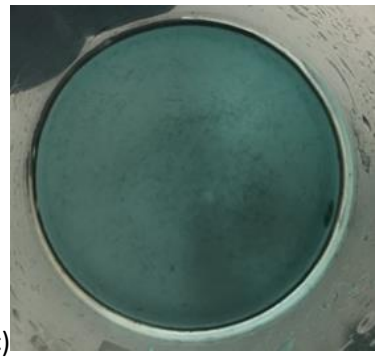

Figure 37. Corrosion in Battery (a) Cathode graphite current collector (b) Catholyte (c) Anolyte

5. Conclusions and Future Work

5.1 Moving Forward with Crosslinking Strategies

Because of the difficulties fabricating a membrane, aim two in the project objectives was unable to be performed. Regardless, it was known from the beginning that this project was extremely ambitious, especially for a single researcher. For future projects, there are multiple directions that crosslinking analyses can be taken. It is still hypothesized that crosslinking across maleic acid is certainly possible. Fischer Esterification is out of the question considering the reaction's water equilibrium properties, but amine and aldehyde crosslinkers might be successful. The chemistry experience or time to perfect the reaction conditions and choose the best crosslinkers was just unavailable in this project. One suggestion would be to have an organic chemist involved in a future project. If any of these reactions worked, it would certainly be preferable to using PSS/PAH. Adding a second polyelectrolyte complicates the system immensely, and there is currently no telling what would happen to ZnO amongst both of them. Additionally, PEC's are much weaker than pure polyelectrolytes when casted. The tensile DMA conducted on dried PSS films would certainly not be at all possible on the PECs created for this study. This is because the early dried PSS films were thin and strong, very similar to the morphology of Nafion. This must be preserved as much as possible.

Retrying UV crosslinking is the most high risk-high reward method to pursue. If successful, the membrane would be able to be casted as a PSS-ZnO composite then crosslinked as a solid membrane. This eliminates any potential changes in the interactions between PSS and ZnO that comes from being in a second solution strictly for a crosslinking reaction. However, these experiments are definitely the most time intensive and complex, requiring an oxygen-depleted environment. Also, a higher wattage UV light would need to be purchased.

However, there is potential with the PSS/PAH PECs crosslinked with glutaraldehyde. The material can crosslink completely in a matter of minutes, and this property should not be taken for granted. However, the fact that electrostatic interactions between polyanion and polycation make up much of the bonding in a PEC makes these materials prone to brittleness from the start. Therefore, improving mechanical strength might be too much of an uphill battle to be worth pursuing. Because glutaraldehyde is somewhat short and straight, it holds PAH layers together extremely tightly, which might contribute to the PEC's brittleness. It may be beneficial to attempt the reaction with other aldehyde crosslinkers that have multiple different structures. Additionally, the PEC's long term chemical stability under a strong acid

is concerning if a membrane deliverable is to supercede Nafion in longevity. As was explained before, Nafion's stability is attributed to its C-F bonds. C-F bonds are the single strongest bonds in organic chemistry, which is why many materials for extreme environments, such as Nafion and Teflon, have many C-F bonds. This may be extremely difficult and a waste of time, but finding a reaction that strips hydrogens off of carbon in favor of fluorines may solve this problem. Alternatively, one may benefit from finding and buying similar polyelectrolytes to PSS and/or PAH that are fluorinated.

Also, if one is interested, research into the previously mentioned popular battery polymers polybenzimidazole and sulfonated polyether ether ketone may be a more prudent decision. There is vastly more cutting-edge literature on the use of polymers similar to these materials for energy technology applications than there is for PSS. This very well could be for good reason.

Finally, there are two promising project directions in battery technology that are outside the scope of this project, and maybe even this lab, but might be useful to consider. The first is the development of batteries that use organic molecules as the anolyte and catholyte charge carriers instead of Nafion, currently spearheaded by Dr. Michael Aziz at Harvard University.[42,43] Since many of these molecules can dissolve in water, the chemical stability requirements for potential membranes are much less strict. This cuts down on battery material costs immensely. Research into the synthesis, characterization, and battery experimentation of high charge-capacity organic molecules might be a better direction than continuing with vanadium. The second direction is the development of membraneless batteries and fuel cells, currently spearheaded by Dr. Daniel Esposito at Columbia University.[44-46] These electrolyzers use unique geometries, flow directions, and properties such as buoyancy to cause separation between anolyte and catholyte solution without the need for a membrane. This latter option is much more feasible for the Peterson lab than the former, since 3D printing is Dr. Esposito's method of rapidly prototyping all battery architectures that are able to be used in experiments.

5.2 Battery Prototype Performance Takeaways

This study was an important first step in the Peterson Lab's expansion into energy technology. While the battery did not perform to the standard of commercial systems, there are various areas where it can be improved in future studies, as explained above. Regardless, even though the performance of the battery itself is not up to par, it is still definitely usable immediately as an experimental tool for membrane studies if it remains consistent. As long as the long term *changes* in voltage and coulombic efficiency can be compared between membranes over multiple charge cycles, the baseline efficiency is of no consequence.

Moreover, before a novel membrane with the necessary properties is successfully created, the battery should be used to compare pure Nafion membranes to Nafion-ZnO hybrids in order to study the effect of nanowires alone on charge transport. Since Nafion dissolves in ethanol, Nafion might be able to electrostatically adhere to ZnO in ethanol solutions before being casted as hybrid membranes. This would be a good way to isolate a single variable, the presence or absence of nanowires, in a way that can be tested as soon as possible. In such a study, the experiments outlined in aim two would also become useful immediately for comparison. Finally, for the lab to continue properly with battery studies, quality battery equipment should be considered for construction, purchase, or collaboration with another lab. This equipment includes: electrochemical glassware (like h-cells), an impedance spectrometer, a diffusion cell, high quality peristaltic pumps, and a battery analyzer (an example would be the ArbinBT 2000, commonly seen in literature).

Once a battery shows acceptable performance, more rigorous charge and discharge tests may be conducted. Specifically, the charging behavior of both solar and wind power may be simulated to charge the battery erratically. Solar energy exhibits gradual increases and decreases in current as the day passes maximum insolation, while wind energy may experience erratic current jumps and drops depending on the weather. Furthermore, failure analysis other than corrosion may be conducted. The battery should be overloaded incrementally up to 400% of its nominal capacity for short bursts, then normal charge cycling should be resumed in order to note any performance damage. Finally, the battery may be put under residential load testing in order to see its response times. Load spikes from literature's home demand models should be scaled down and mimicked on the battery, and changes in current and voltage should be monitored. These models may also be used to predict the required prototype battery scale up necessary to support a single home's demand. Additional electrical circuits required between battery and home, such as DC/AC inverters, power transistors, surge protection equipment, and continuous time control systems, may be constructed and added.

5.3 Future Work: Conduct Alternative Membrane Performance Experiments

Approach

There are multiple measurements that may be taken to gauge the effectiveness of a membrane other than using a prototype battery. Vanadium ion permeability can be tested by determining the diffusion rate of vanadium (IV) ions through UV-Visible spectroscopy, since each oxidation state of vanadium displays a unique color (Figure 17). The membrane would be placed in between two half cells. A solution of 1 M $VOSO_4$, the salt form of vanadium (IV), in 2.5 M sulfuric acid is placed in one half-cell, and a solution of 1 M magnesium sulfate in 2.5 M sulfuric acid is placed in the other. The $MgSO_4$ solution is used to equalize the ionic strengths of the two solutions and to minimize any osmotic pressure effects.[38]

Chemical stability can be determined by measuring membrane mass before and after being suspended in battery solutions containing 1.5-3M V (V). Ultraviolet absorption spectroscopy can also be used to find evidence of oxidized V (IV), an indicator of membrane degradation. Water transport across the membrane can be measured by putting the membrane in between two half cells, both containing Perspex tubes, and checking the water level over time.[8] Ionic conductivity and area resistance can be measured through impedance spectroscopy in an area resistance test cell.[9]

The ion exchange capacity (IEC) of composite membranes can be determined using a titration method.[38] Membranes containing SO_3 groups are titrated with KOH. The salt form of PSS must be soaked in 1M HCl solution to convert it to the acidic, H^+ form. The membrane will then be immersed in a known volume of 0.05 M KOH solution, which will release sulfuric acid protons and increase the pH of the solution. The amount of H^+ released from the membrane will be determined by back titrating the KOH solution with a 0.05 M HCl solution to measure the exact pH change. The membrane will then be washed with distilled water and dried under vacuum. The IEC is calculated as the ratio of the amount of H^+ to the weight of the dried membrane.

Expected Outcomes

The highest performing membranes currently are generally made from PBI. These membranes exhibit an average vanadium ion permeability of 0.004 mol/L after two hours. In contrast, Nafion exhibits an average vanadium ion permeability of 0.06 mol/L after two hours.[38] Also, Nafion's initial weight loss in

5M sulfuric acid is usually around 5%, but weight loss for the latest polymers has dropped down to around 1.5%.[36] The IEC of the Nafion has been measured at 1.5-2 mmol H^+/g, while some membranes have reached levels of 8.5 mmol H^+/g. Finally, water transport per area in most membranes sums to about 0.08 mL/cm^2.[40] It is hypothesized that a PSS/nanowire composite membrane will improve on all of these marks.

5.4 Potential Project Impact

Inorganic nanomaterials in multiple morphologies (rods, sheets, particles) are often studied alone because of their intrinsic mechanical, electrical, and photocatalytic properties. However, they are less often studied in composite materials. Regardless of results, this research could contribute to establishing more intrigue for the electrostatic interactions between inorganic nanomaterials and organic materials. Their possibility to be used as removable templates for self-assembly could be a useful new direction in the study of many different polyelectrolytes.

If an efficient flow battery is able to be constructed with a cost effective, high performance ion exchange membrane, vanadium redox flow battery technology will take another step towards being pushed to the forefront of grid energy storage. More research will need to be done, including follow-up studies to confirm results found in this project and scale up analysis. However, if updated commercial batteries are able to be integrated into renewable energy grids in the near future, renewable energy infrastructure will more easily gain economic prominence as a reliable dominant energy source, thus decreasing the energy sector's carbon footprint. Renewable infrastructure will be able to supply more reliable power with reductions in energy losses and capital costs for renewable utility companies.

6. Appendix

6.1 Reaction Conditions of Fischer Esterification on Maleic Acid

Reaction	Alcohol	Solvent	Acid (excess)	Temp (°C)
1	8.3 mg hydroquinone	Water	5M sulfuric	65
2	7mg glycerol	water	5M sulfuric	65
3	200mg hydroquinone	water	98% sulfuric	65
4	175mg glycerol	water	98% sulfuric	25
5	200mg hydroquinone	water	98% sulfuric	25
6	none	water	98% sulfuric	25
7 (no polymer)	200mg hydroquinone	water	98% sulfuric	25

6.2 Reaction Conditions of Amination on Maleic Acid

Reaction	Amine	Solvent	Catalyst	Temp (°C)
1	400 mg MBCA	water from polymer solution	400 mg DCC	25
2	365 mg (365uL) TEPA	water from polymer solution	400 mg DCC	25
3	400mg MBCA	water from polymer solution	400 mg DCC	50
4	365 mg (365uL) TEPA	water from polymer solution	400 mg DCC	50

7. References:

1. Heard, B. P.; Brook, B. W.; Wigley, T.; Bradshaw, C. Burden of proof: A comprehensive review of the feasibility of 100% renewable-electricity systems. Renewable and Sustainable Energy Reviews 2017, 76, 1122-1133.
2. Ulaganathan, M.; Aravindan, V.; Yan, Q.; Madhavi, S.; Skyllas-Kazacos, M.; Lim, T. M. Recent advancements in all-vanadium redox flow batteries. Advanced Materials Interfaces 2016, 3.
3. Xia, Z.; Ying, L.; Fang, J.; Du, Y.; Zhang, W.; Guo, X.; Yin, J. Preparation of covalently cross-linked sulfonated polybenzimidazole membranes for vanadium redox flow battery applications. J. Membr. Sci. 2017, 525, 229-239.
4. Bi, N.; Zhang, L.; Zheng, Q.; Zhuge, F.; Li, J.; Gao, X. P.; Du, J. Control of ZnO nanowire growth and optical properties in a vapor deposition process. Journal of Materials Science & Technology 2017.
5. Ji, Y.; Tay, Z. Y.; Li, S. F. Y. Highly selective sulfonated poly (ether ether ketone)/titanium oxide composite membranes for vanadium redox flow batteries. J. Membr. Sci. 2017, 539, 197-205.
6. Roe, S.; Menictas, C.; Skyllas-Kazacos, M. A high energy density vanadium redox flow battery with 3 M vanadium electrolyte. J. Electrochem. Soc. 2016, 163, A5028.
7. Prifti, H.; Parasuraman, A.; Winardi, S.; Lim, T. M.; Skyllas-Kazacos, M. Membranes for redox flow battery applications. Membranes 2012, 2, 275-306.
8. Vafiadis, H.; Skyllas-Kazacos, M. Evaluation of membranes for the novel vanadium bromine redox flow cell. J. Membr. Sci. 2006, 279, 394-402.
9. U.S. Internal Revenue Service Residential Renewable Energy Tax Credit | Department of Energy. https://energy.gov/savings/residential-renewable-energy-tax-credit (accessed Sep 23, 2017).
10. Anonymous. Presidential Executive Order on Promoting Energy Independence and Economic Growth. White House Press Releases, Fact Sheets and Briefings / FIND 2017.
11. Parsons, B.; Milligan, M.; Smith, J. C.; DeMeo, E.; Oakleaf, B.; Wolf, K.; Schuerger, M.; Zavadil, R.; Ahlstrom, M.; Nakafuji, D. Y. Grid Impacts of Wind Power Variability: Recent Assessments from a Variety of Utilities in the United States; Preprint; USDOE: United States, Jul 1, 2006.
12. FTHENAKIS, V.; MASON, J. E.; ZWEIBEL, K. The technical, geographical, and economic feasibility for solar energy to supply the energy needs of the US. ENERGY POLICY 2009, 37.

13. Chen, C. L.; Yeoh, H. K.; Chakrabartia, M. H. An enhanced one-dimensional stationary model for the all-vanadium redox flow battery; Proceedings of the 6th International Conference on Process Systems Engineering (PSE ASIA); 2013; Vol. 25, pp 27.
14. Conca, J. Vanadium-Flow Batteries: The Energy Storage Breakthrough We've Needed. Forbes 2016.
15. Hickner, M. A.; Ghassemi, H.; Kim, Y. S.; Einsla, B. R.; McGrath, J. E. Alternative polymer systems for proton exchange membranes (PEMs). Chem. Rev. 2004, 104, 4587-4612.
16. Ashraf Gandomi, Y.; Aaron, D. S.; Mench, M. M. Influence of Membrane Equivalent Weight and Reinforcement on Ionic Species Crossover in All-Vanadium Redox Flow Batteries. Membranes 2017, 7, 29.
17. Wang, W.; Luo, Q.; Li, B.; Wei, X.; Li, L.; Yang, Z. Recent progress in redox flow battery research and development. Advanced Functional Materials 2013, 23, 970-986.
18. Tung, S.; Hwang, B. Synthesis and characterization of hydrated phosphor–silicate glass membrane prepared by an accelerated sol–gel process with water/vapor management. Journal of Materials Chemistry 2005, 15, 3532-3538.
19. Franklin, G. W.; James, C. D. United States Patent 3,282,875, 1966.
20. Teng, H. Overview of the development of the fluoropolymer industry. Applied Sciences 2012, 2, 496-512.
21. Zhou, X. L.; Zhao, T. S.; An, L.; Wei, L.; Zhang, C. The use of polybenzimidazole membranes in vanadium redox flow batteries leading to increased coulombic efficiency and cycling performance. Electrochim. Acta 2015, 153, 492-498.
22. Al Malek, S. A.; Seman, M. A.; Johnson, D.; Hilal, N. Formation and characterization of polyethersulfone membranes using different concentrations of polyvinylpyrrolidone. Desalination 2012, 288, 31-39.
23. Chiang, C.; Wei, M.; Chen, Y.; Yen, P.; Huang, Y.; Chen, J.; Lavastre, O.; Guillaume, H.; Guillaume, D.; Chiou, A. Optical tweezers based active microrheology of sodium polystyrene sulfonate (NaPSS). Optics express 2011, 19, 8847-8854.
24. Yang, D.; Lao, C.; Zewail, A. H. 4D electron diffraction reveals correlated unidirectional behavior in zinc oxide nanowires. Science 2008, 321, 1660-1664.
25. Salarizadeh, P.; Javanbakht, M.; Pourmahdian, S. Enhancing the performance of SPEEK polymer electrolyte membranes using functionalized TiO2 nanoparticles with proton hopping sites. RSC Advances 2017, 7, 8303-8313.
26. Rajabi, H.; Ghaemi, N.; Madaeni, S. S.; Daraei, P.; Astinchap, B.; Zinadini, S.; Razavizadeh, S. H. Nano-ZnO embedded mixed matrix polyethersulfone (PES) membrane: Influence of nanofiller shape on characterization and fouling resistance. Appl. Surf. Sci. 2015, 349, 66-77.
27. Sato, M.; Kawata, A.; Morito, S.; Sato, Y.; Yamaguchi, I. Preparation and properties of polymer/zinc oxide nanocomposites using functionalized zinc oxide quantum dots. European Polymer Journal 2008, 44, 3430-3438.
28. Yamazaki, S.; Ishida, H.; Shimizu, D.; Adachi, K. Photochromic properties of tungsten oxide/methylcellulose composite film containing dispersing agents. ACS applied materials & interfaces 2015, 7, 26326-26332.

29. Rhodes, J. D.; Cole, W. J.; Upshaw, C. R.; Edgar, T. F.; Webber, M. E. Clustering analysis of residential electricity demand profiles. Appl. Energy 2014, 135, 461-471.
30. Anonymous, HOMES SHOW GREATEST SEASONAL VARIATION IN ELECTRICITY USE. States News Service 2013.
31. Randall, T. The Electric-Car Boom Is So Real Even Oil Companies Say It's Coming. Bloomberg.com 2017.
32. Fischer, B. This is what Tesla owners are doing while you sleep. https://blogs.oracle.com/utilities/this-is-what-tesla-owners-are-doing-while-you-sleep (accessed Sep 23, 2017).
33. Twelve economic facts on energy and climate change. *Brookings Institution Reports* 2017.
34. Hong, K.; Kim, S. H.; Yang, C.; Yun, W. M.; Nam, S.; Jang, J.; Park, C.; Park, C. E. Photopatternable Poly (4-styrene sulfonic acid)-wrapped MWNT thin-film source/drain electrodes for use in organic field-effect transistors. *ACS applied materials & interfaces* 2010*, 3*, 74-79.
35. Chen, S.; Krishnan, L.; Srinivasan, S.; Benziger, J.; Bocarsly, A. B. Ion exchange resin/polystyrene sulfonate composite membranes for PEM fuel cells. *Journal of Membrane Science* 2004*, 243*, 327-333.
36. Hosseinzadeh, S.; Pashaei, S.; Moludpoor, N. Fabrication and Characterization of Nanostructured TiO2 and Turmeric Spent Incorporated Polystyrene Hybrid Nano Composites. Iranian Chemical Communication 2017, 5, 16-27.
37. Cho, K. L.; Hill, A. J.; Caruso, F.; Kentish, S. E. Chlorine Resistant Glutaraldehyde Crosslinked Polyelectrolyte Multilayer Membranes for Desalination. *Advanced Materials* 2015*, 27*, 2791-2796.
38. Yuan, Z.; Duan, Y.; Zhang, H.; Li, X.; Zhang, H.; Vankelecom, I. Advanced porous membranes with ultra-high selectivity and stability for vanadium flow batteries. Energy & Environmental Science 2016, 9, 441-447.
39. Sukkar, T.; Skyllas-Kazacos, M. Membrane stability studies for vanadium redox cell applications. J. Appl. Electrochem. 2004, 34, 137-145.
40. Mohammadi, T.; Chieng, S. C.; Kazacos, M. S. Water transport study across commercial ion exchange membranes in the vanadium redox flow battery. J. Membr. Sci. 1997, 133, 151-159.
41. Patel, Bansi R., et al. IEEE Guide for Batteries for Uninterruptible Power Supply Systems. IEEE Standards Association, Stationary Battery Committee of the IEEE Power Engineering Society, 30 Mar. 2006, standards.ieee.org/findstds/standard/1184-2006.html.
42. Huskinson, B., Marshak, M. P., Suh, C., Er, S., Gerhardt, M. R., Galvin, C. J., ... & Aziz, M. J. (2014). A metal-free organic–inorganic aqueous flow battery. Nature, 505(7482), 195.
43. Perry, M. L. (2015). Expanding the chemical space for redox flow batteries. Science, 349(6255), 1452-1452.
44. Davis, J. T., Qi, J., Fan, X., Bui, J. C., & Esposito, D. V. (2018). Floating membraneless PV-electrolyzer based on buoyancy-driven product separation. *International Journal of Hydrogen Energy*, *43*(3), 1224-1238.
45. Esposito, D. V. (2017). Membraneless Electrolyzers for Low-Cost Hydrogen Production in a Renewable Energy Future. Joule.
46. Talabi, O. O., Dorfi, A. E., O'Neil, G. D., & Esposito, D. V. (2017). Membraneless electrolyzers for the simultaneous production of acid and base. Chemical Communications, 53(57), 8006-8009.
47. Anonymous. Conversion of Carboxylic acids to amides using DCC as an activating agent. https://chem.libretexts.org/Core/Organic_Chemistry/Carboxylic_Acids/Reactivity_of_Carboxylic_Acids/Conversion_of_Carboxylic_acids_to_amides_using_DCC_as_an_activating_agent (accessed Apr 12, 2018).

48. Hassan, P. A.; Rana, S.; Verma, G. Making sense of Brownian motion: colloid characterization by dynamic light scattering. Langmuir: the ACS journal of surfaces and colloids 2015, 31, 3.
49. Wikipedia contributors. (2018, January 1). Zeta potential. In Wikipedia, The Free Encyclopedia. Retrieved 01:26, April 20, 2018
50. Kim, J.; Lee, J.; Tak, Y. Relationship between carbon corrosion and positive electrode potential in a proton-exchange membrane fuel cell during start/stop operation. Journal of Power Sources 2009, 192, 674-678.